

## FOR PEER REVIEW - CONFIDENTIAL

**Neuroanatomy of a hydrothermal vent shrimp provides insights into the evolution of crustacean integrative brain centers**

Tracking no: 09-04-2019-RA-eLife-47550

**Impact statement: Using a suite of state-of-the-art neuroanatomical techniques we provide insights into these animal's brain architecture to illustrate possible adaptations to the hydrothermal vent habitat with its extreme physicochemical conditions.****Competing interests:** No competing interests declared**Author contributions:**

Julia Machon: Conceptualization; Data curation; Formal analysis; Validation; Investigation; Visualization; Writing—original draft; Project administration; Writing—review and editing Jakob Krieger: Formal analysis; Investigation; Visualization; Methodology; Writing—original draft; Writing—review and editing Rebecca Meth: Data curation; Formal analysis; Writing—review and editing Magali Zbinden: Conceptualization; Resources; Supervision; Funding acquisition; Investigation; Project administration; Writing—review and editing Juliette Ravaux: Conceptualization; Data curation; Supervision; Funding acquisition; Methodology; Project administration; Writing—review and editing Nicolas Montagné: Conceptualization; Data curation; Supervision; Investigation; Methodology; Writing—review and editing Thomas Chertemps: Conceptualization; Resources; Data curation; Supervision; Investigation; Methodology; Writing—review and editing Steffen Harzsch: Conceptualization; Resources; Formal analysis; Supervision; Writing—original draft; Writing—review and editing

**Funding:**

Deutsche Forschungsgemeinschaft (DFG): Steffen Harzsch, DFG INST 292/119-1 FUGG; Deutsche Forschungsgemeinschaft (DFG): Steffen Harzsch, DFG INST 292/120-1 FUGG The funders had no role in study design, data collection and interpretation, or the decision to submit the work for publication.

**Data Availability:**

The raw data of the micro CT scans and the histological section series will be made public at Morph D Base: <https://www.morphdbase.de/> We will apply for an accession code immediately.

N/A

**Ethics:**

Human Subjects: No Animal Subjects: No

**Information for reviewers (full submissions):**

eLife aims to publish work of the highest scientific standards and importance in all areas of the life and biomedical sciences, from the most basic and theoretical work through to translational, applied and clinical research. Articles must be methodologically and scientifically rigorous, ethically conducted, and objectively presented according to the appropriate community standards.

You will be asked for a general assessment and a summary of any major concerns (ideally in fewer than 500 words), as well as a list of any minor comments (optional). You will also have the opportunity to comment on the statistical rigour of the work (optional).

In your general assessment, please articulate what is exciting and whether the work represents a significant contribution. Please note our guidelines about requests for additional work:

1. We will only request new work, such as experiments, analyses, or data collection, if the new data are essential to support the major conclusions. The authors must be able to do any new work in a reasonable time frame (additional work should be conducted and written up within two months); otherwise, we will usually reject the manuscript.
2. Any requests for new work must fall within the scope of the current submission and the technical expertise of the authors.

Our goal is to make peer review constructive and collaborative: after the reviews have been submitted independently, there is an online discussion between the reviewers in which each reviewer will see the identity of the other reviewers.



## 29 **Abbreviations**

30

31 **(Numbers 1-X)**, cell clusters 1-X; **5HT**, serotonin immunoreactivity; **A1**, antenna 1; **A1l**, lateral  
32 flagellum of antenna 1; **A1INv**, lateral antenna 1 nerve; **A1m**, medial flagellum of antenna 1; **A1mNv**,  
33 medial antenna 1 nerve; **A2**, antenna 2; **A2Nv**, antenna 2 nerve; **AcN**, accessory lobe/neuropil;  
34 **AMPN**, anterior medial protocerebral neuropil; **AnN**, antenna 2 neuropil; **ASTir**, allatostatin-like  
35 immunoreactivity; **b**, base region of the olfactory glomerulus; **bs**, branchiostegite; **c**, cap region of the  
36 olfactory glomerulus; **CA**, cerebral artery; **CA<sub>L</sub>**, lateral cerebral artery; **CA<sub>M</sub>**, median cerebral artery;  
37 **CB**, central body; **DC**, deutocerebrum; **dR**, degenerated rhabdoms; **ENv**, eye nerve; **HN**, hemiellipsoid  
38 body neuropil; **HN<sub>cap</sub>**, hemiellipsoid body cap region; **HN<sub>core</sub>**, hemiellipsoid body core region; **IL**,  
39 intermediate layer; **La**, lamina; **LAN**, lateral antenna 1 neuropil; **IF**, lateral foramen; **Lo**, lobula; **IPC**,  
40 lateral protocerebrum; **maf**, myoarterial formation; **maf<sub>m</sub>**, myoarterial formation muscles **MAN**,  
41 median antenna 1 neuropil; **MAR**, Mid-Atlantic Ridge; **Me**, medulla; **mF**, medial foramen; **mPC**,  
42 median protocerebrum; **MPN**, median protocerebral neuropil; **OA**, ophthalmic artery; **Ob**, onion  
43 bodies; **OBNv**, organ of Bellonci nerve; **oc**, oesophageal connectives; **ocp**, ocular plate; **og**, olfactory  
44 glomerulus; **ON**, olfactory neuropil; **PB**, protocerebral bridge; **pc**, cluster of pigment cells; **PMPN**,  
45 posterior medial protocerebral neuropil; **PNT**, projection neuron tract; **PNTN**, projection neuron tract  
46 neuropil; **PNTCN**, projection neuron tract central neuropil; **PT**, protocerebral tract; **R**, retina; **r**,  
47 rostrum; **sbc**, subcap region of the olfactory glomerulus; **sc**, scaphocerite; **SYNir**, synapsin  
48 immunoreactivity; **T**, tapetum; **T'<sub>d</sub>**, dorsal secondary tendon; **T'<sub>v</sub>**, ventral secondary tendon; **T<sub>a</sub>**,  
49 anterior tendon; **T<sub>d</sub>**, dorsal tendon; **TC**, tritocerebrum; **TM**, terminal medulla neuropil; **TN**,  
50 tegumentary neuropil; **TNv**, tegumentary nerve; **V**, vessel; **VN**, visual neuropils

## 51 Introduction

52

53 The iconic alvinocaridid shrimps were discovered in 1985 during a mission of the deep  
54 submersible vehicle ALVIN (Rona et al., 1986) and are now known to be widely distributed  
55 representatives of the deep hydrothermal vent fauna along the Mid-Atlantic Ridge (MAR;  
56 Desbruyères et al., 2001, 2000; Gebruk et al., 1997; Segonzac et al., 1993). Active vents are dynamic  
57 environments, where geothermally heated seawater, the hydrothermal fluid, discharges from  
58 chimneys and cracks in the seafloor. At the MAR, vents occur from 850 to 4080 m depth and the pure  
59 hydrothermal fluid, which may be up to 350 °C hot, is anoxic, acid, and enriched in potentially toxic  
60 minerals and dissolved gases (Charlou et al., 2010, 2002, 2000). Hydrothermal vent habitats, in  
61 addition to high hydrostatic pressure and the complete absence of sunlight, are characterized by  
62 steep gradients of temperature and concentration of chemicals (Bates et al., 2010; Johnson et al.,  
63 1988, 1986; Le Bris et al., 2005). Vent organisms are well adapted to these physicochemical  
64 conditions, and alvinocaridid shrimps colonize in high abundance the walls of active chimneys, where  
65 the hydrothermal fluid mixes with the surrounding cold (4 °C) and oxygenated seawater. Vent  
66 ecosystems rely on chemoautotrophic bacteria as primary producers, which convert reduced  
67 chemicals through oxidation, thus providing the energy to fix carbon and to produce organic matter  
68 that serves as a nutritional basis for primary consumers (Fisher et al., 2007; Jannasch and Mottl,  
69 1985; Ponsard et al., 2013; Van Dover, 2000).

70 The shrimp *Rimicaris exoculata* (Williams and Rona, 1986) is the most intensely studied vent  
71 crustacean due to its high abundance at most sites along the MAR and its remarkable lifestyle (Fig.  
72 1A,B; Desbruyères et al., 2001; Gebruk et al., 1997; Segonzac et al., 1993; Van Dover et al., 1988).  
73 Specimens of *R. exoculata* are found from 1600 to 4000 m depth (Lunina and Vereshchaka, 2014) and  
74 they form massive aggregations in the vicinity of the chimneys, with up to 3000 ind.m<sup>-2</sup> (Segonzac et  
75 al., 1993). This species is a strict primary consumer, relying on ectosymbiotic bacteria harbored in its  
76 enlarged branchial chambers, through a direct nutritional transfer of bacterial carbon products by  
77 trans-tegumental absorption (Corbari et al., 2008; Petersen et al., 2010; Ponsard et al., 2013; Zbinden  
78 et al., 2004). The associated bacterial metabolic activities include oxidation of sulfide, iron, methane  
79 and hydrogen, suggesting that *R. exoculata* symbionts could have both nutritional and detoxifying  
80 roles for the shrimp (Hügler et al., 2011; Zbinden et al., 2008). Hence, this species is strictly  
81 dependent on hydrothermal fluid emissions to supplement its symbionts with reduced compounds,  
82 and might possess specific sensory abilities for this purpose. Because *R. exoculata* preferentially lives  
83 close to the hydrothermal fluids, the shrimp constantly has to cope with steep temperature gradients

84 ranging approximately from 4 to 40 °C (Cathalot et al., 2018), and its sensory system might be tuned  
85 to efficiently probe this dynamic thermal environment.

86 A fundamental question regarding vent shrimp's environment and lifestyle is how do they  
87 detect hydrothermal emissions and further select their microhabitat. Both abiotic and biotic factors  
88 are important to determine the animal's local distribution at hydrothermal vent sites (Le Bris et al.,  
89 2005; Luther et al., 2001). Several studies showed that *R. exoculata* possesses a range of  
90 morphological, anatomical and physiological adaptations to the hydrothermal environment, related  
91 for instance to ectosymbiosis with bacteria (Casanova et al., 1993; Ponsard et al., 2013; Zbinden et  
92 al., 2004), respiration in hypoxic conditions (Hourdez and Lallier, 2006; Lallier and Truchot, 1997), or  
93 thermal stress (Cottin et al., 2010; Ravaux et al., 2003). However, the sensory mechanisms and  
94 adaptations used by the shrimps to perceive their habitat have only been partially investigated (see  
95 references below) despite their importance in understanding the lifestyle of vent shrimp species and  
96 their long-term evolution.

97 Vision and chemoreception have been proposed to be the major sensory modalities used by  
98 vent shrimp to perceive environmental cues (Chamberlain, 2000; Jinks et al., 1998; Pelli and  
99 Chamberlain, 1989; Renninger et al., 1995). In vent shrimps, the stalked compound eyes that  
100 characterize most malacostracan crustaceans are modified to form enlarged sessile eyes, which in *R.*  
101 *exoculata* are located underneath the dorsal carapace (Chamberlain, 2000; Gaten et al., 1998; O'Neill  
102 et al., 1995; Van Dover et al., 1989). The eyes cannot form images since the ommatidia lack a dioptric  
103 apparatus necessary to refract and focus rays of light, but the retina instead consists of  
104 hypertrophied rhabdoms and a reflective subjacent layer, structures that maximize the absorption of  
105 light. These anatomical features could represent an adaptation to detect very dim light sources. It  
106 was suggested that the animals may perceive the black body radiation emitted by the extremely hot  
107 fluid which exits the chimney (Chamberlain, 2000; Pelli and Chamberlain, 1989; Van Dover et al.,  
108 1989). Furthermore, the animal's antennal appendages respond to sulfide, suggesting that vent  
109 shrimps can detect key chemical components of the hydrothermal fluid (Machon et al., 2018;  
110 Renninger et al., 1995), but sulfide detection is not restricted to vent shrimps since antennal  
111 responses were also recorded from shallow-water Palaemonid shrimp (Machon et al., 2018). From  
112 structural descriptions of their antennae 1 and 2 and chemosensory sensilla, it is not clear whether  
113 their chemosensory system presents specific adaptations related to the hydrothermal environment  
114 (Machon et al., 2018; Zbinden et al., 2017). One specific feature of these organisms is the dense  
115 coverage of their antennal appendages by bacterial communities (Zbinden et al., 2018), whose exact  
116 role remains unknown. Nevertheless, their occurrence on the sensory organs suggests a functional  
117 significance for the shrimp sensory abilities (Zbinden et al., 2018).

118 Crustacean brain structure is best understood in crayfish, crabs, and clawed and spiny  
119 lobsters (reviews e.g. [Derby and Weissburg, 2014](#); [Harzsch and Krieger, 2018](#), [Schmidt, 2016](#)). We are  
120 interested in exploring adaptive changes of crustacean brain structures that have occurred during  
121 their evolutionary radiation into particular habitats and their adoption of specific life styles (e.g.  
122 [Harzsch et al., 2011](#); [Kenning and Harzsch, 2013](#); [Krieger et al., 2015, 2012, 2010](#); [Meth et al., 2017](#)).  
123 Differential investment in certain brain neuropils might reflect the sensory landscape which a certain  
124 crustacean species typically exploits, so that studying an animal's brain anatomy may allow for  
125 predictions related to its ecology and lifestyle ([Sandeman et al., 2014a](#)). For example, in peracarid  
126 and remipedian cave crustaceans, the visual neuropils are absent whereas the central olfactory  
127 pathway is well developed in Remipedia, highlighting that these blind animals may rely on olfaction  
128 as a major sensory modality in their lightless habitat ([Fanenbruck et al., 2004](#); [Fanenbruck and](#)  
129 [Harzsch, 2005](#); [Stegner et al., 2015](#); [Stemme and Harzsch, 2016](#)). In representatives of the genus  
130 *Penaeus*, the olfactory system is moderately developed, while sophisticated antenna 2 neuropils are  
131 present, suggesting that the detection of hydrodynamic stimuli is important for these animals ([Meth](#)  
132 [et al., 2017](#); [Sandeman et al., 1993](#)). Hence, comparing the architecture of the sensory centers  
133 among divergent crustacean lineages, across wide evolutionary distances and across diverse life  
134 styles, can help to understand structural adaptations to specific sensory environments (review in  
135 [Sandeman et al., 2014a](#)). Studying crustaceans from extreme habitats is particularly informative in  
136 this respect ([Ramm and Scholtz, 2017](#); [Stegner et al., 2015](#)). However, the structure of the brain in  
137 vent shrimps remains poorly understood ([Charmantier-Daures and Segonzac, 1998](#); [Gaten et al.,](#)  
138 [1998](#)). Therefore, the present study sets out to provide a detailed description of the architecture of  
139 the *R. exoculata* brain against the background of the extreme conditions that characterize its habitat,  
140 and to ultimately discuss its contribution for crustacean brain evolution.

141 **Results**

142

143 **Gross morphology of the cephalothorax**

144

145 The wide cephalothorax of *Rimicaris exoculata* displays large branchiostegites (*bs*) which  
146 surround voluminous gill chambers (**Fig. 1C**). The animals do not possess eyestalks but bilaterally  
147 paired, wing-shaped eyes with a conspicuous, whitish retina that is fused in the anterior region to  
148 form the ocular plate (*ocp*). The lateral parts of the eye extend further dorsally and towards the  
149 posterior region of the cephalothorax (**Fig. 1C, 2A**). The first pair of antennae (*A1*) is biramous, with  
150 two flagella of similar length (**Fig. 1C**). The second pair of antennae (*A2*) consists of a basal element,  
151 the scaphocerite (*sc*), and a long uniramous flagellum, slightly wider than those of the antennae 1  
152 (**Fig. 1C**). Micro-CT scans show that the brain is located in the anterior region of the cephalothorax,  
153 and receives main sensory afferences from the antenna 1 (*A1Nv*) and antenna 2 (*A2Nv*) nerves  
154 anteriorly, from the eye nerves (*ENv*) posterodorsally, from the tegumentary nerves (*TNv*) laterally,  
155 and from the oesophageal connectives (*oc*) posteriorly (**Fig. 1D**).

156

[Figure 1]

157

158 **Overview of the brain architecture**

159

160 Decapod crustacean brains are subdivided into three successive neuromeres: proto-, deuto-  
161 and tritocerebrum. In *R. exoculata*, these regions form a single, medially located mass (i.e. the  
162 median brain) (**Fig. 1D, 2A**). The visual neuropils are closely associated with the lateral  
163 protocerebrum (*IPC*), at a posterodorsal position (**Fig. 2A**). This arrangement contrasts with other  
164 shallow-water carideans and most decapod crustaceans (see e.g. Cronin and Porter, 2008; Meth et  
165 al., 2017), in which the lateral protocerebrum is located at some distance of the median brain, in  
166 movable eyestalks (**Fig. 2B**). The deutocerebrum (*DC*) is associated with the antenna 1 nerves, and  
167 the tritocerebrum (*TC*) is associated with the antenna 2 nerves (**Fig. 2**). The brain's neuraxis is not  
168 aligned with body axis in *R. exoculata*, but is bent dorsally so that the protocerebrum is situated  
169 posterodorsally to the deutocerebrum (**Fig. 2A**).

170

171 Data from micro-CT scans and aligned serial paraffin sections provided a consistent picture of  
172 the brain anatomy that we compiled in both three-dimensional reconstructions (**Fig. 3A, 4A-D**) and a  
173 schematic drawing of the *R. exoculata* brain (**Fig. 3B, C**). In the following, for simplicity only one brain  
174 hemisphere is described, although mirror symmetrical structures are present in the contralateral  
175 hemisphere.

175 [Figures 2,3,4]

176

177 **Lateral protocerebrum: the visual neuropils**

178

179 *R. exoculata* presents three successive visual neuropils, which are the lamina (*La*), medulla  
180 (*Me*), and lobula (*Lo*), from distal to proximal (**Fig. 3, 4, 5**). The lamina is thin, flattened and elongated  
181 dorsally (**Fig. 4A,D, 5 B-D**). The cell cluster (1) dorsally covers the lamina (**Fig. 3C, 4B,D, 5C**).  
182 Numerous axon bundles from the entire length of the retina (*ENV*) converge onto the lamina (**Fig. 3,**  
183 **4A-D, 5D**). The retina consists of photoreceptor organelles, the rhabdoms (*dR*) (for which the  
184 degradation is ascribed to the damaging exposure to intense light during sampling and manipulation  
185 of the specimens at the surface), which overlie a white layer of reflecting cells, the tapetum (*T*), and  
186 clusters of pigment cells (*pc*) (**Fig. 5D, Fig. 11A; Nuckley et al., 1996; O'Neill et al., 1995**). The medulla  
187 is spherical (**Fig. 3, 4A-D, 5B,C**) and is connected by thin fibers to the lamina (**Fig. 5C**), the lobula (**Fig.**  
188 **5B**) and by a dense fibers tract to the terminal medulla (**Fig. 5B, white arrowhead**). The lobula is  
189 slightly larger than the medulla, and is adjacent to the posterior side of the terminal medulla (*TM*)  
190 (**Fig. 3, 4A-D,F, 5A, 11A**). The merged cell clusters (2) and (3) cannot be clearly separated and cover  
191 both the medulla and the lobula (**Fig. 3C, 4B,D, 5A-C**).

192 [Figure 5]

193

194 **Lateral protocerebrum: the hemiellipsoid body and terminal medulla**

195

196 The lateral protocerebrum dominates the *R. exoculata* brain, with the hemiellipsoid body  
197 (*HN*), the terminal medulla (*TM*), together with the cell clusters (4) and (5) representing about 25 %  
198 of the brain volume. The hemiellipsoid body is well defined, with a voluminous, hemispherical cap  
199 region (*HN<sub>cap</sub>*) located dorsally (**Fig. 3, 4, 5D, 6A-F**) and displaying synapsin immunoreactivity (*SYNir*)  
200 (**Fig. 6G-I**). The core region of the hemiellipsoid body (*HN<sub>core</sub>*) is fused posteriorly with the terminal  
201 medulla (**Fig. 4F, 6B, D,E**). The cap and core regions are separated by an arcuate intermediate layer  
202 (*IL*) (**Fig. 4E, 6A,B,D,E,G-I**) which receives parallel afferent fibers from the terminal medulla anteriorly  
203 (namely the *HN-TM* tract) (**Fig. 3A,B, 4F, 6A-C, black asterisks**) and a massive bundle of neurites from  
204 somata in the cell cluster (5) at the medial side (**Fig. 4E, 5D, 6C-E, white asterisks**). Some of the  
205 intermediate layer fibers display allatostatin-like immunoreactivity (*ASTir*) near the cap region (**Fig.**  
206 **6G**). The intermediate layer is devoid of *SYNir* (**Fig. 6 J**). The cap region is characterized by synaptic  
207 sites forming microglomeruli (**Fig. 6H'**) and is also innervated by serotonergic neurons (**Fig. 6H**). The  
208 cell cluster (5) is voluminous (**Fig. 3C, 4B, 6B-E,I,J**) and contains approximately 30,000 cell somata of

209 the so-called globuli cells (Wolff et al., 2017). The hemiellipsoid body receives input from the  
210 olfactory neuropils *via* the projection neuron tract (*PNT*) in the posterior region (Fig. 3A, 6B, F).

211 The terminal medulla is a large and complex neuropil. Anteriorly, it is shaped like a sphere  
212 (Fig. 3, 4A,C,F, 6A-C), and it connects to the intermediate layer of the hemiellipsoid body *via* the HN-  
213 TM tract (Fig. 3A,D, 4F, 6A-C, *black asterisks*). Posterior to this region, the terminal medulla is large,  
214 crossed by seemingly unstructured networks of fibers (Fig. 3A, 4C,F, 6D-F) and displays SYNir (Fig.  
215 6I,J). It is innervated by neurites from the cell cluster (4) (Fig. 6D, *white arrowhead*), and further  
216 connects again to the intermediate layer of the hemiellipsoid body *via* radiating fiber bundles (Fig.  
217 6E, *black arrowheads*).

218 [Figure 6]

## 220 Median protocerebrum

221  
222 The median protocerebrum (*mPC*) comprises two medially fused neuropils, the anterior  
223 (*AMPN*) and posterior (*PMPN*) medial protocerebral neuropils. The AMPN connects to the terminal  
224 medulla of the lateral protocerebrum anteriorly *via* the protocerebral tract (*PT*) (Fig.3B, 6C,D) and  
225 the PMPN *via* the posterior protocerebral tract (*PPT*), the latter containing neurites with strong  
226 serotonin-immunoreactivity (5HTir) (Fig. 7C) and seemingly interconnecting the terminal medulla of  
227 both hemispheres. Both, the AMPN and PMPN are separated by the unpaired central body neuropil  
228 (*CB*) (Fig. 3), which displays ASTir (Fig. 7B), weak SYNir (Fig. 7A) and strong 5HTir (Fig. 7C). Overall,  
229 the median protocerebrum contains many fibers from serotonergic neurons, partly from the cell  
230 cluster (x) (which likely refers to the cell clusters (12), (13) and (17) according to Sandeman et al.,  
231 1992), which define well the elements of the central complex, i.e. the protocerebral bridge (*PB*) and  
232 the central body (*CB*), and also the posterior region associated to the posterior protocerebral tract.  
233 Posteriorly to the central body, fiber bundles of the projection neuron tracts from both hemispheres  
234 meet in a region with strong SYNir, that we will call the projection neuron tract central neuropil  
235 (*PNTCN*) (Fig. 7A).

236 [Figure 7]

## 238 Deutocerebrum

239  
240 In the deutocerebrum, a paired neuropil with a conspicuous structure is located laterally, the  
241 lobe-shaped olfactory neuropil (*ON*) (Fig. 3, 4A-D, F, 5D, 8A-F). It is composed of approximately 180  
242 wedge-shaped neuropil units, the olfactory glomeruli (*og*), which are arranged radially around the

243 periphery of a non-synaptic core (**Fig. 3B, 4F, 5D, 8A-F**). Each glomerulus shows strong SYNir (**Fig. 8E-**  
244 **F**), as well as ASTir which highlights a subdivision of each glomerulus into a cap (*c*), subcap (*sbc*) and  
245 base (*b*) region (**Fig. 8E'**). The sensory input of the olfactory neuropil comes from the olfactory  
246 sensory neurons innervating the aesthetasc sensilla on the lateral flagellum of the antenna 1. The  
247 somata of olfactory interneurons located in the cell cluster (9/11) innervate fibers to the olfactory  
248 neuropil, some of which display ASTir (**Fig. 8H**). These fibers enter *via* the medial foramen (*mF*) into  
249 the core of the neuropil (**Fig. 8C,E**), from where they target the glomerular base region (**Fig. 8E**), or  
250 cross to the lateral foramen (*lF*) (**Fig. 8A,C,E**) to spread out laterally and innervate the glomerular cap  
251 region (**Fig. 8E**, *white arrowhead*). The medial foramen is also the place where efferent fibers exit  
252 from the olfactory neuropil. These are the axons of the olfactory projection neurons that form the  
253 projection neuron tract (**Fig. 8B,D**). A projection neuron tract neuropil (PNTN) as known from other  
254 decapods (e.g. [Sandeman et al. 1992](#), [Harzsch and Hansson 2008](#), [Krieger et al. 2012](#)) is identifiable  
255 close to the ascending branch of the tract (**Fig. 8E,F**). The projection neuron tract then transverses  
256 the median protocerebrum and projects to the lateral protocerebrum (see above).

257 The lateral antenna 1 neuropil (*LAN*) is located medially to the olfactory neuropil. It is U-  
258 shaped (**Fig. 3, 8A,B,H**) and displays strong SYNir, as well as ASTir, which reveals a transversely  
259 stratified pattern (**Fig. 8G**). This neuropil connects posterodorsally to the median protocerebrum (**Fig.**  
260 **8G,H**).

261 The median antenna 1 neuropil (*MAN*) is small, poorly defined, and located in the center of  
262 the deutocerebrum, below the anterior region of the median protocerebrum and between the paired  
263 lateral antenna 1 neuropils (**Fig. 3A,B**).

264 [Figure 8]

265

## 266 Tritocerebrum

267

268 The tritocerebrum comprises the antenna 2 neuropil (*AnN*), which has a cylindrical shape and  
269 lies in front of the oesophageal connectives (**Fig. 3, 4, 8HA**). SYNir and ASTir show a transversely  
270 stratified pattern within this neuropil (**Fig. 8I**). Poorly differentiated from the antenna 2 neuropil, the  
271 tegumentary neuropil (*TN*) is located posterodorsally (**Fig. 3**).

272

## 273 The organ of Bellonci

274

275 The organ of Bellonci (*OB*) is typical for many crustaceans but its sensory function remains  
276 unclear ([Chaigneau, 1994](#)). In *R. exoculata*, this organ is conspicuous and comprises onion bodies

277 (*Ob*) structures connected to a well-developed nerve tract (*OBV*). The onion bodies are situated on  
278 the anterolateral side of the brain, in front of the hemiellipsoid body (**Fig. 3, 4A-D, 5D, 9A**). They  
279 represent a cluster of about fifty densely packed lobules (**Fig. 9A,B**), many of them containing  
280 elements of granular appearance (**Fig. 9B'**, *white arrowhead*). Some lobules are further located in the  
281 proximal region of *OBV* (**Fig. 9B**). This nerve is large in its proximal region, and progressively tapers  
282 as it draws away from the brain (**Fig. 9A**). Anterodorsally, the nerve extends through the retinal  
283 layers and connects underneath the cuticle of the ocular plate (**Fig. 9C,C'**).

284 [Figure 9]

285

### 286 **The myoarterial formation and cerebral vascular system**

287

288 The myoarterial formation (*maf*) (or *cor frontale*, auxiliary heart) underlies the dorsal  
289 carapace and is located between the paired eyes, above the brain (**Fig. 10A,B,C**). This organ is  
290 voluminous, being almost as long as the elongated retina, and extends ventrally towards the dorsal  
291 region of the brain (**Fig. 10B',C'**). Two adjacent and parallel muscle bundles (*maf<sub>m</sub>*) penetrate through  
292 the myoarterial formation (**Fig. 10A**) and attach to the cuticle *via* tendons located either anteriorly  
293 (*T<sub>a</sub>*) or dorsally (*T<sub>d</sub>*) (**Fig. 10B,C**). Two thinner muscular bundles cross the myoarterial formation in its  
294 middle region, perpendicular to the main adjacent muscles, and are attached both to the dorsal and  
295 ventral cuticle of the cephalothorax, by secondary dorsal and ventral tendons (*T'<sub>d</sub>*, **Fig. 10B,C**; *T'<sub>v</sub>*, **Fig.**  
296 **10B'**).

297 Anteriorly, below the junction of the ocular plate with the dorsal carapace, the myoarterial  
298 formation gives rise to three conspicuous, large cerebral arteries, a central cerebral artery (*CA*) and  
299 two ophthalmic arteries (*OA*), which all make a steep U-turn and extend parallel towards the dorsal  
300 side of the brain (**Fig. 10B,C, arrowhead**). In an anterodorsal position, median to the hemiellipsoid  
301 bodies, the central cerebral artery divides into three smaller arteries, one median (*CA<sub>M</sub>*) and two  
302 lateral ones (*CA<sub>L</sub>*) (**Fig. 10B',C'**). The median artery passes over the brain, between the two spherical  
303 masses of the lateral protocerebrum, and then divides into two branches, one entering the brain  
304 posteriorly, at the level of the median protocerebrum, and a larger one merging with the ventral  
305 region of the myoarterial formation. This suggests a loop system wherein part of the hemolymph in  
306 the cerebral artery goes back into the myoarterial system. The lateral cerebral arteries are coil-  
307 shaped and enter the brain above the insertion of the antenna 1 nerve to target for instance the  
308 olfactory neuropils and the lateral antenna 1 neuropils in the deutocerebrum. The ophthalmic  
309 arteries enter the brain in a posterodorsal position (**Fig. 10C'**) and target the visual neuropils and the  
310 lateral protocerebrum.

311 Anteriorly, below the junction of the ocular plate with the dorsal carapace, the myoarterial  
312 formation gives rise to three conspicuous, large cerebral arteries, a central cerebral artery (CA) and  
313 two ophthalmic arteries (OA), which all make a steep U-turn and extend parallel towards the dorsal  
314 side of the brain (**Fig. 10B,C, arrowhead**). In an anterodorsal position, median to the hemiellipsoid  
315 bodies, the central cerebral artery divides into three smaller arteries, one median ( $CA_M$ ) and two  
316 lateral ones ( $CA_L$ ) (**Fig. 10B',C'**). The median artery passes over the brain, between the two spherical  
317 masses of the lateral protocerebrum, and then divides into two branches, one entering the brain  
318 posteriorly, at the level of the median protocerebrum, and a larger one merging with the ventral  
319 region of the myoarterial formation. This suggests a loop system wherein part of the hemolymph in  
320 the cerebral artery goes back into the myoarterial system. The lateral cerebral arteries are coil-  
321 shaped and enter the brain above the insertion of the antenna 1 nerve to target for instance the  
322 olfactory neuropils and the lateral antenna 1 neuropils in the deutocerebrum. The ophthalmic  
323 arteries enter the brain in a posterodorsal position (**Fig. 10C'**) and target the visual neuropils and the  
324 lateral protocerebrum.

325 The cerebral vascular system of *R. exoculata* is considerably developed, with blood vessels  
326 supplying all brain neuropils and cell clusters, as in other crustaceans, including large vessels that  
327 irrigate the visual neuropils (**Fig. 5A,C**), the deutocerebrum (**Fig. 8B**) and the lateral protocerebrum  
328 (**Fig. 9B,B'**). The Azan staining reveals pink-to-purple cerebral arteries that enter the brain (CA) (**Fig.**  
329 **5C,D, 8A,B, 10A**), and orange vessels inside the brain (V) (**Fig. 5A,C, 8B, 9B**).

330 [Figure 10]

331

### 332 **Comparisons of the olfactory system and the higher integrative centers with other crustaceans**

333

334 **Table 1** presents a comparison of aesthetasc and olfactory neuropil characteristics in  
335 different taxa of crustaceans. The number of olfactory glomeruli in *R. exoculata* fits within the range  
336 displayed by other decapods, but their unitary volume is in the lower range, leading to relatively  
337 small olfactory neuropils (excluding the fibrous core) compared to other species (**Table 1, Fig. 11e**). In  
338 contrast, the higher integrative centers (i.e. the hemiellipsoid body and the medulla terminalis,  
339 associated to cell cluster 5) are especially well-developed in *R. exoculata* compared to other  
340 crustaceans and in relation to the relative size of the olfactory neuropils (**Fig. 11**). As an example,  
341 from relative volumes obtained from 3D reconstructions, the higher integrative centers in *R.*  
342 *exoculata* occupy approximately 25 % of the total brain volume, similarly to the caridean shrimp  
343 *Palaemon elegans* (22 %) but twice more than in the giant robber crab *Birgus latro* (13 %), whereas

344 their olfactory neuropils are respectively almost twice (4.2 %) and six (17 %) times more voluminous  
345 than those of *R. exoculata* (2.7 %).

346 [Table 1]

347 [Figure 11]

348

## 349 Discussion

350

### 351 General remarks

352

353 The emblematic alvinocaridid shrimp *Rimicaris exoculata* is an endemic species to  
354 hydrothermal vent habitats, well adapted to these deep sea environments with peculiar  
355 physicochemical conditions. The present study sets out to gain insights into adaptations to specific  
356 features of the vent habitat (e.g. low ambient light levels and steep variations of chemical  
357 concentrations). The analysis of the brain architecture in *R. exoculata* aims to highlight relative  
358 investments into certain neuronal subsystems, in relation with the animal's habitat and lifestyle. The  
359 general anatomy of the brain of *R. exoculata* corresponds in many aspects to the ground pattern of  
360 the malacostracan crustacean brain (Kenning et al. 2013), including the subdivision into proto-,  
361 deuto- and tritocerebrum, the location of main nerves and the presence of distinct cell clusters.  
362 However, the brain of *R. exoculata* also exhibits morphological differences to other malacostracans,  
363 especially at the level of the lateral protocerebrum. The organ of Bellonci is especially conspicuous  
364 (also observed by Charmantier-Daures and Segonzac, 1998), but its sensory function remains elusive.  
365 In the following, we will focus on the structure of major sensory centers (i.e. the visual system, the  
366 olfactory system and the higher integrative centers). We will also discuss the evolution of the  
367 hemiellipsoid bodies as higher integrative brain centers, which are remarkable in *R. exoculata*. We  
368 will begin our account by addressing the neurovascular system that supplies the brain.

369

### 370 The neurovascular system

371

372 In crustaceans, the neurovascular system has been described mainly in crayfish (Chaves da  
373 Silva et al., 2012; Scholz et al., 2018), crabs (McGaw, 2005; McGaw and Reiber, 2002; Sandeman and  
374 Callan 1967) and spiny lobsters (Steinacker, 1979) (reviews in McMahon, 2001; Steinacker, 1979,  
375 1978; Wilkens, 1999). The brain and eyes are supplied in hemolymph *via* the anterior aorta system,  
376 which originates antero-medially from the heart and runs between the stomach and the dorsal  
377 integument (Scholz et al., 2018). Anteriorly, a dilatation of the anterior aorta, the myoarterial  
378 formation (Scholz et al., 2018; also named the cor frontale in e.g. McGaw, 2005; Steinacker, 1978)  
379 which functions as an auxiliary heart, pumps the hemolymph specifically towards the anterior part of  
380 the central nervous system. In malacostracan crustaceans, the myoarterial formation above the brain  
381 gives rise to a descending cerebral artery, which supplies the median brain, and to two ophthalmic  
382 arteries that turn laterally and extend into the eyestalks to supply the visual neuropils (Chaves da

383 [Silva et al., 2012](#); [McGaw, 2005](#); [Scholz et al., 2018](#)). In *R. exoculata*, consistent with the absence of  
384 eyestalks, the myoarterial formation and its arteries differ in shape, size and position from those  
385 previously described in other malacostracans. Among the potential corollaries for the pronounced  
386 neurovascular system in *R. exoculata*, one is the more efficient hemolymph pumping to the brain. In  
387 crustaceans, the perfusion of the brain is modulated by physiological or environmental factors, such  
388 as hypoxia ([Reiber and McMahon, 1998](#)). Because the pure hydrothermal fluid is anoxic, the mixing  
389 of the fluid with the surrounding seawater can create hypoxic conditions for vent animals ([Childress  
390 and Fisher, 1992](#); [Schmidt et al., 2008](#)). Known adaptations to hypoxia in vent crustaceans include an  
391 hemocyanin with a higher affinity for oxygen compared to shallow-water species ([Chausson et al.,  
392 2004](#); [Lallier and Truchot, 1997](#); [Sanders et al., 1988](#)). A very pronounced capillary network was also  
393 observed in hydrothermal vent alvinellid polychaetes ([Hourdez and Lallier, 2006](#)). Accordingly, the  
394 pronounced myoarterial formation and large cerebral arteries in *R. exoculata* could represent a  
395 particularly efficient system for oxygen delivery to the brain to cope with low availability of oxygen.

396

#### 397 **A visual system adapted to a dim light environment**

398

399 [Van Dover and co-workers \(1989\)](#) described the *R. exoculata* eyes as a pair of large anteriorly  
400 fused organs that underlie the transparent dorsal carapace of the cephalothorax and demonstrated  
401 the presence of rhodopsin-like visual pigments in high quantity, with a maximum absorption at 500  
402 nm. Subsequent analyses showed that the eyes comprise a smooth cornea located above a dense  
403 layer of hypertrophied rhabdoms, under which a white layer of reflective cells, the tapetum, is  
404 located and maximizes the absorption of light by the photoreceptors ([Chamberlain, 2000](#); [Jinks et al.,  
405 1998](#); [Nuckley et al., 1996](#); [O'Neill et al., 1995](#)). These elements of the retina were all discernible in  
406 our histological sections, although the rhabdoms were strongly degenerated, a process ascribed to  
407 the damaging exposure to intense light during sampling ([Herring et al., 1999](#); [Johnson et al., 1995](#)).  
408 The eyes of *R. exoculata* lack the dioptric apparatus which characterizes the ommatidia of  
409 compound eye pelagic and shallow water crustaceans and thus cannot form images ([Chamberlain,  
410 2000](#); [Jinks et al., 1998](#); [Nuckley et al., 1996](#); [O'Neill et al., 1995](#)), but their highly sensitive naked  
411 retina seems adapted for the detection of low ambient light levels, to the detriment of spatial  
412 resolution ([Chamberlain, 2000](#); [Van Dover et al., 1989](#)).

413 In malacostracan crustaceans, the visual input from the compound eyes is processed by a  
414 suite of retinotopic visual neuropils, usually but not exclusively located within the moveable  
415 eyestalks (**Fig. 2B**) ([Strausfeld, 2012](#), [Loesel et al., 2013](#)). The absence of eyestalks of *R. exoculata*  
416 coincides with a strong size reduction and fusion of the visual neuropils with the median brain (**Fig.**

417 **2A).** Nevertheless, already [Charmantier-Daures and Segonzac \(1998\)](#) and [Gaten and co-workers](#)  
418 [\(1998\)](#) differentiated three visual neuropils in *R. exoculata*, namely the lamina, medulla, and lobula,  
419 as in the ground pattern of the Malacostraca. However, in *R. exoculata* these neuropils are located  
420 posterodorsally to the enlarged lateral protocerebrum. The dorsal expansion of the flattened lamina,  
421 that extends in parallel to the retina, suggests a retinotopic projection of photoreceptor input onto  
422 the lamina which may allow the animals to extract directional information from light sources above.  
423 In the medulla, immunohistochemistry revealed an outer layer (which is also faintly visible in  
424 histological sections), suggesting a subdivision of the medulla into an outer and inner region, as seen  
425 in crayfish ([Strausfeld and Nässel, 1981](#)). No such stratification was observed for the lobula, and  
426 synapsin immunoreactivity was weak in this most proximal neuropil, although in malacostracans with  
427 well-developed compound eyes, the lobula displays numerous, neurochemically diverse strata (e.g.  
428 *Brachyura* and *Anomura*, [Harzsch and Hansson, 2008](#); [Krieger et al., 2012, 2010](#); [Wolff et al., 2012](#);  
429 *Astacidea*, [Polanska et al., 2007](#); *Dendrobranchiata*, [Meth et al., 2017](#); *Stomatopoda*, [Strausfeld,](#)  
430 [2005](#)). The simplified structure of the lobula which in other malacostracans plays a role in motion  
431 detection ([Strausfeld, 2012](#)) may mirror the inability of the eye to form images. Also, the lobula plate,  
432 a fourth visual neuropil present in several malacostracan taxa (e.g. *Brachyura* and *Anomura*,  
433 [Bengochea et al., 2017](#); [Harzsch and Hansson, 2008](#); [Krieger et al., 2012, 2010](#); [Sztarker et al., 2009](#);  
434 *Dendrobranchiata*, [Meth et al., 2017](#); *Stomatopoda*, [Strausfeld, 2005](#); *Leptostraca*, [Kenning et al.,](#)  
435 [2013](#); *Isopoda*, [Kenning and Harzsch, 2013](#); [Sinakevitch et al., 2003](#)) could not be identified in *R.*  
436 *exoculata*. The lobula plate has been suggested to mediate optokinetic control, necessary to track  
437 moving objects (e.g. conspecifics, preys, predators) ([Sztarker et al., 2005](#)). Such a role is consistent  
438 with the loss of the lobula plate in *R. exoculata*, which lacks the realization of image formation,  
439 necessary for tracking moving objects.

440 Many eyeless representatives of Crustacea have partially or totally lost their central visual  
441 pathways (e.g. *Peracarida*, [Ramm and Scholtz, 2017](#); [Stegner et al., 2015](#); *Cephalocarida*, [Elofsson and](#)  
442 [Hessler, 1990](#); [Stegner and Richter, 2011](#); *Remipedia*, [Fanenbruck et al., 2004](#); *Mystacocarida*,  
443 [Brenneis and Richter, 2010](#)), potentially under the selective pressure that favors a reduction of these  
444 nervous tissues to limit the amount of energy expended on their function ([Klaus et al., 2013](#); [Moran](#)  
445 [et al., 2015](#); [Niven and Laughlin, 2008](#)). Contrary, the fact that neuronal elements indicative for a  
446 functional visual system are present in *R. exoculata* must mean that there is light to exploit as an  
447 environmental cue. Also, the unusual nature of the visual system of *R. exoculata* suggests that it  
448 exploits a specific type of signal. One prominent hypothesis refers to the thermal black body  
449 radiation emitted by the hot hydrothermal fluid at the chimney's exit with a temperature of up to  
450 350 °C, which peaks in the infrared but part of its spectrum extends into the visible light ([Pelli and](#)

451 Chamberlain, 1989; Van Dover et al., 1996, 1988; Van Dover and Fry, 1994). The ability to localize this  
452 radiation could serve both to attract the shrimp to optimal areas for supplying its symbionts with  
453 vital, reduced compounds of the hydrothermal fluid, and to allow avoidance of scorching fluid (Van  
454 Dover et al., 1989). Visual cues other than thermal radiation are likely to be also exploited by *R.*  
455 *exoculata*, related to turbulence, mixing and precipitation, such as chemi-, crystallo-, tribo- and sono-  
456 luminescence, for which the emission spectra lie between 450-800 nm (Reynolds and Lutz, 2001;  
457 Tapley et al., 1999; Van Dover et al., 1996; Van Dover and Fry, 1994; White, 2000; White et al., 2002).

458

## 459 **The olfactory system**

460

461 Two modes of chemoreception, linked to distinct chemosensory pathways, are distinguished  
462 in malacostracan crustaceans (Derby and Weissburg, 2014; Schmidt and Mellon, 2010): olfaction,  
463 which is mediated by the aesthetasc sensilla located on the lateral flagellum of the antenna 1, and  
464 distributed chemoreception, which is mediated by the bimodal chemo- and mechanosensory sensilla  
465 located mainly on all antennal appendages, the mouthparts, and the walking appendages (Garm et  
466 al., 2005, 2003; Garm and Watling, 2013; Mellon, 2014, 2012; Schmidt and Gnatzy, 1984). *R.*  
467 *exoculata* presents aesthetascs in similar number and dimensions to other caridean representatives  
468 (**Table 1**), as well as several bimodal sensilla with different morphologies on the antennal  
469 appendages (Zbinden et al., 2017).

470 Olfaction has been extensively studied in malacostracans (e.g. Ache, 2002; Derby and  
471 Weissburg, 2014; Schmidt and Mellon, 2010), and the central olfactory pathway has received much  
472 attention in crustacean neuroanatomy (e.g. Blaustein et al., 1988; Harzsch and Krieger, 2018;  
473 Kenning et al., 2013; Kenning and Harzsch, 2013; Krieger et al., 2015, 2012, 2010; Sandeman et al.,  
474 1992; Schachtner et al., 2005; Schmidt and Mellon, 2010). The afferent olfactory input from the  
475 olfactory sensory neurons innervating the aesthetascs targets the conspicuous olfactory neuropils,  
476 which are lobe-shaped and bilaterally arranged in the deutocerebrum (**Fig. 8A-F**). They are composed  
477 of spherical or cone-shaped dense synaptic neuropils, namely the olfactory glomeruli, which are  
478 radially arranged around the periphery of a core of non-synaptic fibers. The olfactory glomeruli are  
479 subdivided into a cap, subcap and base regions in several decapod taxa (e.g. Harzsch and Krieger,  
480 2018; Schachtner et al., 2005; Schmidt and Ache, 1997). The glomeruli of *R. exoculata* appear to  
481 conform to this principle design, with an identical subdivision (**Fig. 8E'**). Although the number of  
482 olfactory glomeruli is in the same range to that of its close relative *Palaemon elegans*, the olfactory  
483 neuropils of *R. exoculata* are relatively small in terms of volume and not overly developed compared  
484 to other species (**Table 1** and **Fig. 11**). Hence, the dimensions and structural complexity of the

485 olfactory neuropils in *R. exoculata* do not suggest, judging from comparative brain anatomy, that the  
486 loss of the eye's capacity to form images is compensated by sophisticated olfactory abilities.

487       Efficient olfactory abilities would have been especially relevant to probe the chemical  
488 environment of *R. exoculata*, which is dynamic, with strong concentration variations of hydrothermal  
489 fluid chemicals as the hydrothermal fluid dilutes with the surrounding seawater. Sulfide and other  
490 chemicals could serve as highly important environmental cues for *R. exoculata* (Renninger et al.  
491 1995, Machon et al. 2018) to locate active edifices as optimal areas to supply its chemoautotrophic  
492 symbionts with reduced compounds. However, sulfide detection is likely mediated by distributed  
493 chemoreception, or both distributed chemoreception and olfaction, rather than exclusively olfaction,  
494 as it can be detected by the flagella of the antenna 2 which does not bear aesthetascs (Machon et al.,  
495 2018). Olfaction is also involved in the recognition of conspecifics (Thiel and Breithaupt, 2011) and  
496 the localization of sexual partners (Wyatt, 2014), but there is to date no detailed information on the  
497 inter-individual interactions in and out of the swarms of *R. exoculata*. The detection of chemical cues  
498 produced by bacteria could also appear especially relevant since the sensory antennal appendages of  
499 vent shrimp are often covered by a dense bacterial layer, whose roles are unknown yet (Zbinden et  
500 al. 2018).

501

#### 502 **Evolution of higher integrative brain centers: the hemiellipsoid body**

503

504       Malacostracan crustaceans display a rich repertoire of complex behavioral patterns related  
505 to finding food, shelter and mating partners, kin recognition and brood care, as well as orientation  
506 and homing. Decapod crustaceans are also known for complex social interactions such as communal  
507 defensive tactics, the occupation of common shelters, cooperative behavior during long-distance,  
508 offshore seasonal migration and the establishment of dominance hierarchies (Breithaupt and Thiel,  
509 2011; Derby and Thiel, 2014; Duffy and Thiel, 2007; Thiel and Watling, 2015). Because such complex  
510 behaviors most likely involve elements of learning and memory, higher integrative brain centers are  
511 suggested to provide the neuronal substrate for more sophisticated processing underlying such  
512 behaviors (review in Sandeman et al., 2014a). Such centers receive input exclusively from second or  
513 higher order neurons but not from any primary sensory afferents (i.e. from the peripheral nervous  
514 system) and contain interneurons responding to the stimulation of several different sensory systems.  
515 In the malacostracan brain, the (bilaterally paired) terminal medulla, hemiellipsoid body, and  
516 accessory lobe seem to function as higher integrative centers, all three distinct neuropil areas which  
517 display a high level of complexity and are notable for their substantial volume (Sandeman et al.,  
518 2014a). The terminal medulla and the closely associated hemiellipsoid body, are targeted by axons

519 of the olfactory projection neurons as output pathway of the olfactory neuropil and accessory lobe  
520 (where present; reviews [Derby and Weissburg, 2014](#); [Harzsch and Krieger, 2018](#); [Schmidt, 2016](#)).  
521 Because of these anatomical relation, evolutionary ([Sullivan and Beltz, 2004, 2001](#)) and functional  
522 considerations ([Harzsch and Krieger, 2018](#); [Sandeman et al., 2014a](#); [Strausfeld, 2012](#)) have focused  
523 on possible roles of these centers in higher order olfactory processing. In addition to the olfactory  
524 projection neuron axons, the terminal medulla also receives input from the visual neuropils in several  
525 malacostracans (reviewed in [Sandeman et al., 2014a](#)). A specific type of local interneurons associated  
526 to the medulla terminalis and the hemiellipsoid body are the parasol cells ([Mellon and Alones, 1997](#);  
527 [McKinzie et al., 2003](#); [Mellon et al., 1992](#); [Mellon, 2000](#); [Mellon et al., 1992](#)) which respond to  
528 olfactory, tactile, and visual stimuli, thus highlighting their role as elements in higher order  
529 integration ([Mellon and Alones, 1997](#); [Mellon, 2003, 2000](#); [Mellon and Wheeler, 1999](#)). Recent  
530 evidence obtained from a brachyuran crab suggests an involvement of the crustacean hemiellipsoid  
531 body/terminal medulla complex in memory processes ([Maza et al., 2016](#)). Furthermore, considering  
532 anatomical similarities of the crustacean hemiellipsoid body and insect mushroom body, [Wolff and](#)  
533 [co-workers \(2017\)](#) suggested an involvement in place memory.

534 [Figure 12]

535

536 During the evolutionary elaboration of malacostracan brains, substantial modifications  
537 occurred related to the relative proportion of secondary sensory input and investment in size of the  
538 various higher integrative centers (**Fig. 11**; [Harzsch and Krieger, 2018](#); [Sandeman et al., 2014a](#)).  
539 Because the terminal medulla has a highly complex and highly variable structure, being composed of  
540 several, partly confluent neuropil lobes with heterogeneous appearance containing both coarse and  
541 fine fibers (e.g. [Blaustein et al., 1988](#)), its architecture so far has not been studied in a comparative  
542 context. We will focus in the following on the hemiellipsoid body whose structure is somewhat easier  
543 to grasp (**Fig. 11**). In its simplest form, the hemiellipsoid body consists of a volume of fine neuropil  
544 with little texture that is closely associated with the terminal medulla (**Fig. 11, 12**). Such a phenotype  
545 is for example common in leptostracans, the presumably most basal branch of the Malacostraca  
546 ([Kenning et al., 2013](#)), but also in representatives of the Dendrobranchiata ([Meth et al., 2017](#);  
547 [Sullivan and Beltz, 2004](#)), and several Brachyura ([Krieger et al., 2010, 2012b, 2015](#)). Isopoda as  
548 representatives of the Peracarida also feature simple, dome-shaped hemiellipsoid bodies (**Fig. 11, 12**;  
549 [Kenning and Harzsch, 2013](#); [Stemme and Harzsch, 2016](#)) whereas in Amphipoda ([Ramm and Scholtz,](#)  
550 [2017](#)) and blind groups of peracarids from relict habitats ([Stegner et al., 2015](#)), this center is poorly  
551 developed and may be entirely missing. A more complex phenotype features a separation of the  
552 hemiellipsoid body into two separated areas, an architecture present for example in the spiny  
553 lobsters (neuropils I and II, [Blaustein et al., 1988](#)), the crayfish *Procambarus clarkii* and *Orconectes*

554 *rusticus* (neuropil I and II, Sullivan and Beltz, 2001), and *Cherax destructor* (HBI and HBII, Sullivan and  
555 Beltz, 2005). The clawed lobster *Homarus americanus* also features two neuropil units, but these are  
556 stacked on top of each other as cap and core neuropils separated by an intermediate, non-synaptic  
557 layer (Sullivan and Beltz, 2001). Additional differences exist between the crayfish and the clawed  
558 lobster concerning the areas that are targeted by the axons of the projection neurons. (Mellon et al.,  
559 1992; Mellon et al., 1992; Sullivan and Beltz, 2005, 2001). Hemiellipsoid bodies with a cap/core  
560 structure separated by an intermediate layer are also present in the brains of marine (Krieger et al.,  
561 2012b) and terrestrial hermit crabs of the taxon Coenobitidae, *Coenobita clypeatus* (Harzsch and  
562 Hansson, 2008; Polanska et al., 2012; Wolff et al., 2012) and *Birgus latro* (Krieger et al., 2010). These  
563 animals all display a large hemiellipsoid body with a peripheral, dome-shaped cap neuropil enclosing  
564 two dome-shaped core neuropil areas Core 1 and Core 2 (Fig. 10, 11). Their hemiellipsoid body is  
565 associated with several thousands of small, intrinsic neurons (Harzsch and Hansson, 2008; Krieger et  
566 al., 2010) The cap and core neuropils are separated by intermediate layers formed by the neurites of  
567 these intrinsic interneurons and the afferents of the projection neuron tract in a rectilinear  
568 arrangement (Wolff et al., 2012).

569 In the hemiellipsoid bodies of the stomatopod crustaceans *Gonodactylus bredenii* (Sullivan  
570 and Beltz, 2004) and *Neogonodactylus oerstedii* (Wolff et al., 2017), the cap/core motif is modified  
571 such that the cap layer (termed “calyx” in Wolff et al., 2017) is much thinner than the core neuropil  
572 and that the cluster of intrinsic neurons expands over much of the surface of the cap neuropil. The  
573 additional stalked neuropils in the lateral protocerebrum of *N. oerstedii* (Wolff et al., 2017) will not  
574 be discussed here for simplicity. In *Stenopus hispidus* (Stenopodidea), the hemiellipsoid body appears  
575 very complex in structure, with apparently three distinct lobular neuropils (Sullivan and Beltz 2004;  
576 Krieger et al., unpublished). The hemiellipsoid body in the caridean species *P. elegans* and  
577 *Palaemonetes pugio* also presents three lobular neuropils, two of which present a cap layer and one  
578 or two core regions, and a third neuropil without clear subdivision (Fig. 11D, Fig. 12; Sullivan and  
579 Beltz 2004). The hemiellipsoid body of *R. exoculata* in many aspects, closely corresponds to the  
580 cap/core layout although it is slightly simpler than in Coenobitidae with only one core neuropil,  
581 similar to the arrangement observed in *H. americanus* (Sullivan and Beltz, 2001) (Fig. 12).

582 In summary, the hemiellipsoid body displays more structural variations across the  
583 Malacostraca than many other elements of the crustacean brain areas which led Sandeman and co-  
584 workers (2014) to note that, within the Malacostraca, several different evolutionary trajectories are  
585 present to increase their brain’s capacity for integrating olfactory and multimodal stimuli. This  
586 diversity masks common motifs of hemiellipsoid body architecture, explaining why genealogical  
587 relationships of the crustacean and insect protocerebral multimodal centers have been discussed

588 controversially for many years (reviews e.g. [Loesel et al., 2013](#); [Sandeman et al., 2014b](#); [Strausfeld,](#)  
589 [2012, 2009, 1998](#)). Latest evidence suggests that, despite many morphological differences, these  
590 protocerebral structures of insects and crustaceans nevertheless share common architectural,  
591 physiological and neurochemical features suggesting a homology of their very basic neuronal  
592 circuitry ([Brown and Wolff, 2012](#); [Maza et al., 2016](#); [Wolff et al., 2012, 2017](#); [Wolff and Strausfeld,](#)  
593 [2015](#)).

594

#### 595 **Possible functions of the hemiellipsoid body: new lesson from *R. exoculata*?**

596

597         Because the projection neuron tract provides a massive input to the lateral protocerebrum,  
598 recent comparative considerations have suggested that the structural elaboration and size of  
599 hemiellipsoid bodies largely mirror the importance of the central olfactory pathway in a given brain,  
600 thus emphasizing their role in higher order olfactory processing (e. g. [Harzsch and Krieger, 2018](#);  
601 [Sandeman et al., 2014](#)). Along these lines, [Harzsch and Hansson \(2008\)](#) and [Krieger and co-workers](#)  
602 [\(2010\)](#) noted that in representatives of the Coenobitidae, the architectural complexity and volume of  
603 the olfactory neuropil closely correlates to that of the hemiellipsoid body. The comparative plates  
604 (**Fig. 11 and 12**) demonstrate that *R. exoculata* dramatically deviates from this pattern in that their  
605 disproportionately large hemiellipsoid body contrasts with an inconspicuous, small olfactory neuropils.  
606 The observation that visual input is likely to also play a subordinate role in these animals compared  
607 to shallow-water relatives with fully developed compound eyes makes us suggest that in *R.*  
608 *exoculata*, their impressive hemiellipsoid body must fulfil additional functions in addition of higher  
609 order sensory processing. Discussing anatomical similarities of the crustacean hemiellipsoid body and  
610 insect mushroom body, [Wolff and co-workers \(2017a\)](#) suggested for these two neuropils a role in  
611 place memory, based on observations that insects with elaborate navigational skills display elaborate  
612 mushroom bodies. Considering recent experiments that suggest an involvement of the crustacean  
613 hemiellipsoid body/terminal medulla-complex in memory processes ([Maza et al., 2016](#)), we here  
614 propose that the hemiellipsoid body in *R. exoculata* is involved in the formation of place memory.  
615 This hypothesis is further supported by the presence of serotonergic tracts within the hemiellipsoid  
616 bodies (**Fig. 6H**), since serotonin has a function for place memory and learning in the mushroom  
617 bodies of *Drosophila melanogaster* (e.g. [Sitaraman et al., 2008](#)). Spiny lobsters *Panulirus argus* are  
618 renowned for their extensive offshore migrations and their ability to orient accurately towards their  
619 home sites over long distances by using the direction of water movement (surge) caused by wave  
620 action, learned local structural features, and geomagnetic cues for navigation (reviewed in [Sandeman](#)  
621 [et al., 2014](#)). Using a GPS-based telemetric system, giant robber crabs, *Birgus latro*, were shown to  
622 form route memories and may use path integration as navigation strategy and in translocation

623 experiments were shown to be capable of homing over large distances (Krieger et al., 2012a). The  
624 above mentioned crustacean species display impressive hemiellipsoid bodies. For survival in the  
625 extreme, lightless habitat of *R. exoculata*, an excellent place memory may be essential for avoiding  
626 the dangerously hot vent chimneys and memorizing emission sites of hydrothermal fluids rich in  
627 those chemicals on which their endosymbiont bacteria depend.

628

## 629 **Conclusion**

630

631 Our observations of the general brain architecture of *R. exoculata* highlight several specific  
632 peculiarities, which could be related to adaptations to the specific sensory landscape of the vent  
633 habitat. The well-developed neurovascular system could be particularly efficient for brain  
634 oxygenation, to cope with the low availability of oxygen in the close surroundings of active chimneys.  
635 The conservation of the visual pathway and neuropils in a mostly aphotic environment suggests that  
636 vision nevertheless is a relevant sense for vent shrimp, although they lack effective motion detection  
637 abilities. The olfactory system does not present specific traits and is probably not a dominant sensory  
638 modality in this shrimp unlike what has been proposed so far. On the other hand, the higher  
639 integrative centers are especially well-developed, and the disproportionally large hemiellipsoid  
640 bodies could be involved in complex integrative processes such as place memory, which could be a  
641 primary navigational cue. Overall, vent shrimp appear to be especially interesting models to  
642 investigate both sensory adaptations to peculiar environmental conditions, and the evolution of the  
643 sensory centers among Crustacea.

## 644 **Materials and Methods**

645

### 646 **Animal collection and fixation procedures**

647

648 Specimens of alvinocaridid shrimp *R. exoculata* (Williams and Rona, 1986) were collected on  
649 the TAG vent site (MAR, 26°08'N-44°49'W, 3600 m depth) during the BICOSE 2018 cruise on the  
650 Research Vessel 'Pourquoi Pas?'. Animals were sampled with the suction device of the Diving Support  
651 Vessel 'Nautille 6000', and recovered at their *in situ* pressure using the PERISCOP isobaric recovery  
652 device (Shillito et al., 2008). Immediately after retrieval, specimens were dissected to remove the  
653 hepatopancreas prior to fixation. The specimens for histology and x-ray micro-computed tomography  
654 (*micro-CT*) scans were stored in Bouin's fixative (10 % formaldehyde, 5 % glacial acetic acid in  
655 saturated aqueous picric acid) at 4 °C until use. The specimens for immunohistochemistry were  
656 fixed 24 to 48 h in 4 % formaldehyde (FA) in 0.1 M Phosphate buffered saline (PBS) at 4 °C for 24 h,  
657 and then stored in 0.1 M PBS with NaN<sub>3</sub> at 4 °C until use. All specimens were sexed using the sexual  
658 dimorphism from the second pair of pleopods. Specimens are females for all micro-CT and histology  
659 experiments, and are both females and males for immunohistochemistry.

660 Caridean shallow water shrimp *Palaemon elegans* (Rathke, 1837) were collected from Saint-  
661 Malo Bay (France; 48°64'N,-2°00'W), in January 2018, using a shrimp hand net. Specimens were  
662 dissected and fixed as described above. Protocols for other species are described in the following:  
663 *Nebalia herbstii*, Kenning et al., 2013; *Penaeus vannamei*, Meth et al., 2017; *Saduria entomon*,  
664 Kenning and Harzsch, 2013; *Carcinus maenas*, Krieger et al., 2012; *Birgus latro*, Krieger et al., 2010.

665

### 666 **Histology**

667

668 The heads of Bouin-fixed animals were dehydrated in a graded series of ethanol and  
669 embedded in paraffin wax mixed with 5 % beeswax. Serial sections (7 µm) were taken in the frontal  
670 or sagittal plane with a microtome (Leica RM 2145; Leica Microsystems, Wetzlar, Germany). The  
671 sections were stained with Azan-novum according to Geidies using standard protocols (Welsch and  
672 Mulisch, 2010).

673

### 674 **Immunohistochemistry**

675

676 The brains of fixed animals (4 % FA) were dissected in PBS 0.1 M, pH 7.4, embedded in low-  
677 gelling agarose (Cat. A9414; Sigma-Aldrich Chemie GmbH, Munich, Germany) and sectioned (100 µm)

678 with a vibratome (Hyrax V50; Carl Zeiss, Oberkochen, Germany). The sections were preincubated for  
679 1.5 h in PBT (PBS + 0.3 % Triton X-100 + 1 % bovine serum albumine) to improve antibody  
680 penetration. Two sets of combinations of markers were used: 1. anti-synapsin+ anti-allatostatin+  
681 nuclear marker; 2. anti-synapsin + anti-serotonin+ nuclear marker. The sections were first incubated  
682 overnight in the primary antisera at room temperature. The antisera used were: monoclonal anti-  
683 SYNORF1 synapsin antibody (DSHB, 3C11; from mouse); polyclonal anti-A-allatostatin antiserum (A-  
684 type Dip-allatostatin I; Jena Bioscience, abd-062; from rabbit); polyclonal anti-Serotonin (5-HT,  
685 Immunostar, Cat. No 20080, from rabbit, igG). After incubation, the sections were washed in several  
686 changes of PBT for 1 h and afterwards incubated in the secondary antibodies (anti IgGs) conjugated  
687 to Alexa Fluor 488 (Alexa Fluor 488 goat anti-rabbit IgG Antibody, invitrogen, Molecular Probes) and  
688 Cy3 (Cy3-conjugated AffiniPure Goat Anti-Mouse IgG Antibody, Jackson ImmunoResearch  
689 Laboratories Inc.) overnight at room temperature. Additionally, HOECHST 33258 (Cat. 14530; Sigma-  
690 Aldrich Chemie GmbH, Munich, Germany) was used as a nuclear marker to show the cell clusters.  
691 The sections were finally washed in several changes of PBT for 2 h and mounted in Mowiol 4-88 (Cat.  
692 0713.2; Carl Roth, Karlsruhe, Germany).

693

#### 694 **Antibody specificity**

695

##### 696 • Synapsin

697 The monoclonal anti-SYNORF1 synapsin antibody (DSHB Hybridoma Product 3C11; anti  
698 SYNORF1 as deposited to the DSHB by E. Buchner) was raised against a *Drosophila melanogaster*  
699 GST-synapsin fusion protein and recognizes at least four synapsin isoforms (70, 74, 80 and 143 kDa)  
700 in western blots of *D. melanogaster* head homogenates (Klagges et al., 1996). Sullivan and co-  
701 workers (2007) showed a single band at ca. 75 kDa in a western blot analysis of crayfish  
702 homogenates. Harzsch and Hansson (2008) conducted a western blot analysis comparing brain tissue  
703 of *D. melanogaster* and the hermit crab *Coenobita clypeatus* (Anomura, Coenobitidae). The SYNORF1  
704 serum provided identical results for both species and it stained one strong band between 80 and 90  
705 kDa and a second weaker band slightly above 148 kDa, suggesting that the epitope that SYNORF1  
706 recognizes is strongly conserved between *D. melanogaster* and *C. clypeatus* (see Harzsch and  
707 Hansson, 2008). Similar to the fruit fly, the antibody consistently labels brain structures in other  
708 major subgroups of the malacostracan crustaceans (e.g., Beltz et al., 2003; Harzsch et al., 2002, 1999,  
709 1998; Krieger et al., 2012) in a pattern that is consistent with the assumption that this antibody labels  
710 synaptic neuropils in crustaceans. The antibody also labels neuromuscular synapses in Crustacea and  
711 *Drosophila* (Harzsch et al., 2002).

712

713       • Allatostatin

714           The A-type allatostatins represent a large family of neuropeptides that were first identified  
715 from the cockroach *Diploptera punctata*; they additionally share the C-terminal motif -YXFGLamide  
716 (Christie et al., 2010; Nässel and Homberg, 2006; Stay et al., 1995; Stay and Tobe, 2007). In the shore  
717 crab *Carcinus maenas* (Brachyura), almost 20 native A-type allatostatin-like peptides were identified  
718 from extracts of the thoracic ganglia (Duve et al., 1997). Shortly afterwards, various other A-type  
719 allatostatin-like peptides were isolated from the Eastern Crayfish *Orconectes limosus* (Astacida;  
720 Dirksen et al., 1999). Meanwhile, A-type allatostatin peptides have been discovered in a wide range  
721 of malacostracan crustaceans, including Brachyura (e.g. Huybrechts et al., 2003), Astacida (e.g. Cape  
722 et al., 2008), the prawns *Penaeus monodon* (Duve et al., 2002), *Macrobrachium rosenbergii* (Yin et  
723 al., 2006) and also in the shrimp *Penaeus vannamei* (Ma et al., 2010; Meth et al., 2017). Christie  
724 (2016) identified a total of 29 peptides with the C-terminal motif, -YXFGLamide, in the latest analysis  
725 on the peptidome of the shore crab. The polyclonal rabbit allatostatin antiserum used in the present  
726 study was raised against the *Diploptera punctata* A-type Dip-allatostatin I,APSGAQRLYGFLamide,  
727 coupled to bovine thyroglobulin using glutaraldehyde (Vitzthum et al., 1996). It has previously been  
728 used to localize A-type allatostatin-like peptides in crustacean and insect nervous systems (e.g.,  
729 Kreissl et al., 2010; Polanska et al., 2012). In the following, the term “allatostatin-like  
730 immunoreactivity” is used to indicate that the antibody most likely binds to various related peptides  
731 within this peptide family.

732

733       • Serotonin

734           The antiserum against serotonin (ImmunoStar Incorporated; Cat. No. 20080, Lot No. 541016)  
735 is a polyclonal rabbit antiserum raised against serotonin coupled to bovine serum albumin (BSA) with  
736 paraformaldehyde. The antiserum was quality control tested by the manufacturer using standard  
737 immunohistochemical methods. According to the manufacturer, staining with the antiserum was  
738 completely eliminated by pretreatment of the diluted antibody with 25 µg of serotonin coupled to  
739 BSA per ml of the diluted antibody. We repeated this control with the serotonin-BSA conjugate that  
740 was used for generation of the antiserum as provided by ImmunoStar (Cat. No. 20081, Lot No.  
741 750256; 50 µg of lyophilized serotonin creatinine sulfate coupled to BSA with paraformaldehyde).  
742 Preadsorption of the antibody in working dilution with the serotonin-BSA conjugate at a final  
743 conjugate concentration of 10 µg/ml at 4 °C for 24 h completely blocked all immunolabeling. We  
744 performed an additional control and preadsorbed the diluted antiserum with 10 mg/ml BSA for 4 h at  
745 room temperature. This preadsorption did not affect the staining, thus, providing evidence that the  
746 antiserum does not recognize the carrier molecule alone. The manufacturer also examined the cross  
747 reactivity of the antiserum. According to the data sheet, with 5 µg, 10 µg, and 25 µg amounts, the

748 following substances did not react with the antiserum diluted to 1:20,000 using the horse radish  
749 peroxidase (HRP) labeling method: 5-hydroxytryptophan, 5-hydroxyindole-3-acetic acid, and  
750 dopamine.

751

## 752 **Imaging**

753

754 The brain tissues processed for immunofluorescence were viewed with a Leica TCS SP5II  
755 confocal laser-scanning microscope equipped with DPSS, Diode- and Argon-lasers and operated by  
756 the Leica “Application Suite Advanced Fluorescence” software package (LASAF) (Leica Microsystems,  
757 Wetzlar, Germany). Digital images were processed with Adobe Photoshop CS4 or ImageJ. Only global  
758 picture enhancement features (brightness and contrast) were used.

759 The head tissues processed for histology were viewed with a Nikon Eclipse 90i upright  
760 microscope and bright-field optics (Nikon, Amstelveen, Netherlands). Serial images using a mounted  
761 digital camera (Nikon DS-Fi3) were aligned manually with the 3D-reconstruction software Amira 5.6.0  
762 (FEI Visualization Science Group, Burlington, VT, USA).

763 For frontal and sagittal sections, dorsal is always towards the top.

764 In the figures, the following color-coded abbreviations were used to identify the markers:  
765 SYN, synapsin (*magenta*); AstA, allatostatin (*green*); 5HT, serotonin (*green*); NUC, nuclear counter  
766 stain (*cyan*). Colors were chosen according to Color Universal Design for accessibility to colorblind  
767 readers.

768

## 769 **X-ray micro-computed tomography**

770

771 Micro-CT scans were performed using an X-ray microscope (Xradia MicroXCT-200; Carl Zeiss  
772 Microscopy GmbH, Jena, Germany) that uses a 90-kV/8-W tungsten X-ray source and switchable  
773 scintillator-objective lens units as described by [Sombke et al. \(2015\)](#). The heads of fixed animals  
774 (Bouin) were contrasted in iodine solution (2 % iodine resublimated (Cat. #X864.1; Carl Roth GmbH,  
775 Karlsruhe, Germany) in 99.5 % ethanol), critical point-dried using a fully automatic critical point dryer  
776 Leica EM CPD300 (Leica Microsystems, Wetzlar, Germany) and scanned dry (scan medium air).  
777 Tomography projections were reconstructed using the reconstruction software XMReconstructor  
778 (Carl Zeiss Microscopy GmbH, Jena, Germany), resulting in image stacks (DICOM format) with a pixel  
779 size of about 5.8  $\mu\text{m}$  for the 4 $\times$  objective and 1.9  $\mu\text{m}$  for the 10 $\times$  objective.

780

## 781 **3D Reconstruction**

782

783 The 3D reconstructions of brain and substructures are based on manual segmentation based  
784 on image stacks obtained either by the micro-CT scans or by the alignment of serial histological  
785 sections, and were performed using the software Amira (FEI Visualization Science Group, Burlington,  
786 VT, USA) as described in [Sombke et al., 2015](#). The computed 3D surfaces were slightly smoothed.

787

## 788 **Nomenclature**

789

790 The neuroanatomical nomenclature used in this manuscript for neuropils, clusters of cell  
791 bodies and tracts is based on [Sandeman et al., 1993](#) and [Richter et al. \(2010\)](#) with some  
792 modifications adopted from [Krieger et al. \(2015\)](#) and [Loesel et al. \(2013\)](#). The term “visual neuropils”  
793 is used instead of “optic neuropils” as suggested by [Krieger et al. \(2015\)](#). The terms lamina, medulla  
794 and lobula are used for the visual neuropils instead of the lamina ganglionaris, medulla externa and  
795 medulla interna ([Harzsch, 2002](#)). The term “olfactory neuropil” refers to the deutocerebral  
796 chemosensory lobe in [Loesel et al. \(2013\)](#) and [Krieger et al. \(2015\)](#). The olfactory globular tract is  
797 named the projection neuron tract (PNT) according to [Loesel et al. \(2013\)](#). Cell clusters are referred  
798 by their given numbers in parentheses. Because no border was detectable between the cell clusters  
799 (9) and (11), they are collectively referred as cluster (9/11) ([Krieger et al., 2015](#)), and accordingly are  
800 the cell clusters (2) and (3), referred as cluster (2/3). (x) refers likely to the fusion of the cell clusters  
801 (12), (13) and (17) according to the nomenclature from [Sandeman et al., 1992](#).

802

## 803 **Calculations**

804

805 For the volumes of the HN-TM (hemiellipsoid body and terminal medulla complex in both  
806 hemispheres) and the olfactory neuropils relative to the total brain volume, measurements were  
807 made from 3D reconstructions of the structures from micro-CT scans using the Amira software. For  
808 the brain volume, the brain was delimited where the antennal nerves and the oesophageal  
809 connectives separate from the syncerebrum. Additionally, for *P. elegans*, the volume of the eyestalks  
810 which does neither contain any neuropil nor any cell cluster was subtracted to the total brain  
811 volume, so that the comparison with *R. exoculata* (which does not possess eyestalks) was relevant.  
812 Same calculations were applied on the *Birgus latro* data from [Krieger et al. 2010](#).

813 The number of globuli cells (i.e. cell somata in the cell cluster (5)) was determined by  
814 estimation of the globuli cell densities in the cell cluster (5), and the total volume of one cell cluster  
815 (5). The globuli cell densities were estimated by direct counting of the somata within 0.02 to 0.04  
816 mm<sup>2</sup> paraffin sections of 0.007 mm thickness ( $1.3 \times 10^{-4}$  to  $2.8 \times 10^{-4}$  mm<sup>3</sup>), with a density estimated to

817 be approximately  $1.3 \times 10^6$  globuli cells per  $\text{mm}^3$ . The total volume of one cell cluster (5) was  
818 calculated from 3D-reconstructions with the Amira software.

819 For the volume of the olfactory neuropils and the number of olfactory glomeruli,  
820 measurements and estimations were made from sections revealed by synapsin immunoreactivity as  
821 described in [Beltz et al. \(2003\)](#).

822 **Acknowledgements**

823

824           The authors thank the chief scientist of the Bicose 2018 cruise (M-A. Cambon), as well as the  
825 captain and crew of the research vessel “Pourquoi pas?” and the HOV Nautille team for sampling the  
826 hydrothermal shrimp. We thank B. Shillito and L. Amand for the use of the PERISCOP device, the  
827 Ifremer for providing pictures of *R. exoculata* swarms, E. Becker for the histological sections, P. O. M.  
828 Steinhoff for critical point drying the samples, M. Charmantier for feedback on the organ of Bellonci,  
829 and C. Wirkner and S. Scholz for their advice on the myoarterial formation.

830           This study was financed by an incoming international stipend from the University of  
831 Greifswald, the German Science Foundation; Grant number: DFG INST 292/119-1 FUGG, DFG INST  
832 292/120-1 FUGG, and a fellowship grant from InterRidge.

833

834

835 **Competing interests**

836

837           The authors declare there are no competing interests.

838 **Figure legends**

839

840 **Figure 1. The Alvinocaridid vent shrimp *Rimicaris exoculata*.**

841 **A,B.** Swarms of thousands of *R. exoculata* individuals are crowded along the walls of black smoker  
842 hydrothermal vents at the TAG vent site (3600 m depth), Mid-Atlantic Ridge  
843 (©IFREMER/Nautilé6000, BICOSE 2018 cruise). **C.** Dorsal view of the cephalothorax of *R. exoculata*,  
844 showing voluminous gill chambers covered by the branchiostegites, dorsal eyes (i.e. ocular plate)  
845 with two elongated retinæ fused in the anterior region, and sensory appendages (antennae 1 and 2).  
846 Scale bar = 5 mm. **D.** Black-white inverted image from an X-ray micro-CT scan showing a dorsal  
847 overview of the *R. exoculata* cephalothorax, with 3D reconstruction of the brain and associated  
848 nerves.

849

850 **Figure 2. Comparative brain overview in Caridean vent and shallow-water species.**

851 Lateral sketches of the brains of the vent shrimp *Rimicaris exoculata* (**A**) and the closely-related  
852 shallow-water shrimp *Palaemon elegans* (**B**), showing the brain position within the cephalothorax,  
853 the position of the main nerves and the subdivision of the brain into three neuromeres called proto-,  
854 deuto- and tritocerebrum, plus the visual neuropils. In contrast to *P. elegans*, *R. exoculata* does not  
855 possess eyestalks and the visual neuropils are fused to the median brain, in a dorsoposterior position  
856 behind the lateral protocerebrum.

857

858 **Figure 3. Overall organization of the brain of *R. exoculata*.**

859 3D reconstruction (**A**) and schematic representations (**B,C**) of the brain and neuropils of *R. exoculata*  
860 viewed from a dorsal, slightly anterior direction. The open white arrow points towards anterior of the  
861 body axis. In **C**, the clusters of cell somata associated with the neuropils are shown. The 3D  
862 reconstruction is based on an image stack obtained by serial sectioning of paraffin-embedded  
863 material.

864

865 **Figure 4. Additional views of the brain morphology in *R. exoculata*.**

866 **A-D.** 3D reconstruction of the brain of *R. exoculata* in anterior-left (**A,B**) and left (**C, D**) views, based  
867 on an image stack obtained by serial sectioning of paraffin-embedded material. **B** and **D** include the  
868 cell clusters. The brain orientation is sketched in the bottom right corners. **E,F.** Lateral sections of the  
869 brain of *R. exoculata* from micro-CT scans (black-white inverted images). The section's positions are  
870 depicted in the bottom left corners. White asterisk in **E** indicates the entrance of axons from the cell

871 cluster (5) into the hemiellipsoid body. Black asterisk in **F** indicates the tract connecting the anterior  
872 region of the terminal medulla to the hemiellipsoid body. The open white arrows point towards  
873 anterior of the body axis. Scale bars = 100  $\mu\text{m}$ .

874

875 **Figure 5. Lateral protocerebrum: the visual neuropils.**

876 **A-C.** Frontal histological sections in the posterior region of the brain, from anterior to posterior,  
877 showing the visual neuropils, associated cell clusters, and part of the vascular system. The white  
878 arrow head in **B** shows the fiber tract connecting the medulla to the terminal medulla. **D.** Sagittal  
879 histological section of the brain, showing the eye nerve fibers projecting from the anterodorsal retina  
880 to the lamina. White asterisks indicate the entrance of axons from the cell cluster (5) into the  
881 hemiellipsoid body intermediate layer. The open white arrow points towards anterior of the body  
882 axis. The section's positions are sketched in the bottom left corners. Scale bars = 100  $\mu\text{m}$ .

883

884 **Figure 6. Lateral protocerebrum: the hemiellipsoid body and the terminal medulla**

885 **A.** 3D reconstruction of the lateral protocerebrum (right hemisphere), viewed from an anterior-left  
886 perspective, based on an image stack obtained by X-ray micro-CT scan. A conspicuous arcuate tract  
887 connects the anterior region of the terminal medulla to the cap region of the hemiellipsoid body (see  
888 also in **C**). **B.** Schematic representation of the lateral protocerebrum (right hemisphere), viewed from  
889 the left. Dotted lines indicate the section's position in **C-F**. **C-F.** Frontal histological sections of the  
890 lateral protocerebrum, from anterior to posterior. The hemiellipsoid body and the terminal medulla  
891 receive axons from the cell somata in the cell cluster (5) (*white asterisks*, **C-E**) and (4) (*white*  
892 *arrowhead*, **D**). An arcuate tract connects the terminal medulla to the cap region of the hemiellipsoid  
893 body in the anterior region (*black asterisk*, **C**). The terminal medulla also connects to the  
894 hemiellipsoid body in the middle region, *via* arborizing fibers (*black arrowheads*, **E**). The projection  
895 neuron tract enters the hemiellipsoid body in the posterior region (**F**). **G-J'.** Horizontal sections of the  
896 lateral protocerebrum, from dorsal to ventral, double or triple-labeled for synapsin immunoreactivity  
897 (SYN, *magenta*), allatostatin-like immunoreactivity (AST) or serotonin immunoreactivity (5HT) (both  
898 showed in *green*), and a nuclear marker (NUC, *cyan*). The inset (H') shows an enlargement of the  
899 hemiellipsoid body neuropil cap region, with microglomeruli. The section's positions are sketched in  
900 the bottom right corners. Black and white open arrows point towards anterior of the body axis. Scale  
901 bars = 100  $\mu\text{m}$  (except in H', scale bar = 50  $\mu\text{m}$ ).

902

903 **Figure 7. Median protocerebrum.**

904 **A-C.** Black-white inverted images of horizontal sections of the median protocerebrum labeled for  
905 synapsin immunoreactivity (**A**), allatostatin-like immunoreactivity (**B**) or serotonin immunoreactivity  
906 (**C**). The section's positions are sketched in the bottom right corners. Black arrows point towards  
907 anterior of the body axis. Scale bars = 100  $\mu\text{m}$ .

908

909 **Figure 8. Deutocerebrum and tritocerebrum.**

910 **A,B.** Overview of the deutocerebrum and tritocerebrum (frontal histological sections). **A** is anterior to  
911 **B**. **C,D.** Sagittal histological sections of the olfactory neuropils. **E,F.** Horizontal sections of the  
912 olfactory neuropil, triple-labeled for synapsin immunoreactivity (SYN, *magenta*), allatostatin-like  
913 immunoreactivity (AST, **E,E'**) or serotonin immunoreactivity (5HT, **F**) (*green*), and a nuclear marker  
914 (NUC, *cyan*). **G.** Horizontal section of the transversely stratified (*white asterisk*) lateral antenna 1  
915 neuropil, double-labeled for synapsin immunoreactivity (SYN, *magenta*) and allatostatin-like  
916 immunoreactivity (AST, *green*). **H.** Sagittal histological section of the tritocerebrum, and part of the  
917 deutocerebrum and median protocerebrum. **I.** Horizontal section of the transversely stratified  
918 antenna 2 neuropil, double-labeled for synapsin immunoreactivity (SYN, *magenta*) and allatostatin-  
919 like immunoreactivity (AST, *green*). The section's positions are sketched in the bottom corners. Black  
920 and white open arrows point towards anterior of the body axis. Scale bars = 100  $\mu\text{m}$ .

921

922 **Figure 9. The organ of Bellonci.**

923 **A-B'.** Frontal histological sections of the anterior region of the brain, showing conspicuous onion  
924 body-structures from which a nerve tract emanates (**A,B**), and which are seemingly closely associated  
925 to the cerebral vascular system (**B'**). The section's positions are sketched in the bottom left corners.  
926 **C.** Anterodorsolateral overview of the cephalothorax from micro-CT scan. Asterisks indicate the  
927 position where the organ of Bellonci nerve connects to the cuticle beneath the anterior region of the  
928 ocular plate. **C'** shows a 3D reconstruction of the brain and the organ of Bellonci nerve in this region.  
929 White arrow points towards anterior of the body axis. Scale bars = 100  $\mu\text{m}$ .

930

931 **Figure 10. The myoarterial formation and cerebral vascular system.**

932 **A.** Frontal histological section of the myoarterial formation located between the bilateral retina and  
933 above the visual neuropils. The section's position is sketched in the bottom left corner. Scale bar =  
934 100  $\mu\text{m}$ . **B,C.** 3D reconstruction of the myoarterial formation (*orange*), part of the cerebral vascular  
935 system (*blue* and *cyan*) and the brain (*yellowish*), from lateral (**B**) and anterolateral (**C**) views, in the

936 cephalothorax. **B'** and **C'** show higher magnifications of the cerebral vascular system. Dotted arrows  
937 indicate structures inside the brain. Open white arrows point towards anterior of the body axis.

938

939 **Figure 11. Comparison of the higher integrative centers and olfactory neuropils in several**  
940 **representatives of Malacostraca displayed at the same scale.**

941 Sections of the higher integrative centers (i.e. hemiellipsoid body and terminal medulla) (**A-G**) and  
942 horizontal sections of the olfactory neuropil (**a-g**) labeled with different sets of antibodies (see  
943 below), in several malacostracan species: *Nebalia herbstii* (**Aa**, Leptostraca, from Kenning et al.,  
944 2013), *Penaeus vannamei* (**Bb**, Dendrobranchiata, from Meth et al., 2017), *Saduria entomon* (**Cc**,  
945 Isopoda, from Kenning and Harzsch, 2013), *Palaemon elegans* (**Dd**) and *Rimicaris exoculata* (**Ee**)  
946 (Caridea, this study), *Carcinus maenas* (**Ff**, Brachyura, from Krieger et al., 2012) and *Birgus latro* (**Gg**,  
947 Anomala, from Krieger et al., 2010).

948 Markers: **a**, SYNir; **B**, SYNir + RFair; **b**, SYNir + RFair + NUC; **Cc**, SYNir + 5HTir; **A,d,e**, SYNir + ASTir;  
949 **D,E,F-g**, SYNir + ASTir + NUC.

950 *ASTir*, allatostatin-like immunoreactivity (*green*); *NUC*, nuclear marker (*cyan*); *RFair*, RFamide-like  
951 immunoreactivity (*green*); *SYNir*, synapsin immunoreactivity (*magenta*); *5HTir*, serotonin  
952 immunoreactivity (*green*).

953

954 **Figure 12. Structure of the hemiellipsoid body in several representatives of Malacostraca.**

955 The sketches of the hemiellipsoid body structure are displayed in relative size and include  
956 representatives of Leptostraca (*Nebalia herbstii*, Kenning et al., 2013), Stomatopoda  
957 (*Neogonodactylus oerstedii*, Wolff et al., 2017; *Gonodactylus bredini*, Sullivan and Beltz, 2004),  
958 Dendrobranchiata (*Penaeus vannamei*, Meth et al., 2017; *Penaeus duorarum*, Sullivan and Beltz,  
959 2004), Caridea (*Rimicaris exoculata* and *Palaemon elegans*, this study; *Palaemonetes pugio*, Sullivan  
960 and Beltz, 2004), Stenopodidea (*Stenopus hispidus*, Sullivan and Beltz, 2004 and Krieger et al.  
961 unpublished), Achelata (*Panulirus argus*, Blaustein et al., 1988), Homarida (*Homarus americanus*,  
962 Sullivan and Beltz, 2001), Astacida (*Procambarus clarkii*, Sullivan and Beltz, 2001), Anomala (*Birgus*  
963 *latro*, Krieger et al., 2010); *Coenobita clypeatus*, Wolff et al., 2012; *Pagurus bernhardus*, Krieger et al.,  
964 2012), Brachyura (*Carcinus maenas*, Krieger et al., 2012), Euphausiacea (*Meganyctiphanes norvegica*,  
965 unpublished), Thermosbaenacea (*Tethysbaena argentarii*, Stegner et al., 2015), Amphipoda  
966 (*Orchestia cavimana* and *Niphargus puteanus*, Ramm and Scholtz, 2017), Mictacea (*Mictocaris*  
967 *halope*, Stegner et al., 2015), Spelaeogriphacea (*Spelaeogriphus lepidops*, Stegner et al., 2015) and  
968 Isopoda (*Saduria entomon*, Kenning and Harzsch, 2013; *Idotea emarginata*, Stemme et al., 2014).  
969 Sketches were made from sections stained using antibody raised against synapsin, except *N.*

970 *puteanus* (antibody raised against tubulin), *M. norvegica*, *P. argus* and *O. cavimana* (histological  
971 sections), and *N. herbstii* (optical section). The symbol “?” indicates that the presence of a  
972 hemiellipsoid body is uncertain. The phylogram showing phylogenetic relationships of malacostracan  
973 crustaceans is modified from [Harzsch and Krieger 2018](#) (therein modified from [Sandeman et al.,](#)  
974 [2014](#), as compiled after [Richter and Scholtz, 2001](#); [Scholtz and Richter, 1995](#); [Wirkner and Richter,](#)  
975 [2010](#)).

976

977 **References**

978

979 **Ache BW.** 2002. Crustaceans as animal models for olfactory research. In: Wiese K (Ed.), Crustacean  
 980 Experimental Systems in Neurobiology. Springer, Berlin, Heidelberg, pp. 189–199.  
 981 [doi:10.1007/978-3-642-56092-7\\_11](https://doi.org/10.1007/978-3-642-56092-7_11)

982 **Bates AE,** Lee RW, Tunnicliffe V, Lamare MD. 2010. Deep-sea hydrothermal vent animals seek cool  
 983 fluids in a highly variable thermal environment. *Nature Communications* **1**:14.  
 984 [doi:10.1038/ncomms1014](https://doi.org/10.1038/ncomms1014)

985 **Beltz BS,** Kordas K, Lee MM, Long JB, Benton JL, Sandeman DC. 2003. Ecological, evolutionary, and  
 986 functional correlates of sensilla number and glomerular density in the olfactory system of  
 987 decapod crustaceans. *Journal of Comparative Neurology* **455**:260–269. [doi:10.1002/cne.10474](https://doi.org/10.1002/cne.10474)

988 **Bengochea M,** Berón de Astrada M, Tomsic D, Sztarker J. 2017. A crustacean lobula plate:  
 989 Morphology, connections, and retinotopic organization. *Journal of Comparative Neurology*  
 990 **526**:109–119. [doi:10.1002/cne.24322](https://doi.org/10.1002/cne.24322)

991 **Blaustein DN,** Derby CD, Simmons RB, Beall AC. 1988. Structure of the brain and medulla terminalis  
 992 of the spiny lobster *Panulirus argus* and the crayfish *Procambarus clarkii*, with an emphasis on  
 993 olfactory centers. *Journal of Crustacean Biology* **8**:493–519. [doi:10.1163/193724088X00341](https://doi.org/10.1163/193724088X00341)

994 **Breithaupt T,** Thiel M, editors. 2011. Chemical Communication in Crustaceans. New York: Springer-  
 995 Verlag.

996 **Brenneis G,** Richter S. 2010. Architecture of the nervous system in Mystacocarida (Arthropoda,  
 997 Crustacea)—an immunohistochemical study and 3D reconstruction. *Journal of morphology*  
 998 **271**:169–189.

999 **Brown S,** Wolff G. 2012. Fine structural organization of the hemiellipsoid body of the land hermit  
 1000 crab, *Coenobita clypeatus*. *Journal of Comparative Neurology* **520**:2847–2863.  
 1001 [doi:10.1002/cne.23058](https://doi.org/10.1002/cne.23058)

1002 **Cape SS,** Rehm KJ, Ma M, Marder E, Li L. 2008. Mass spectral comparison of the neuropeptide  
 1003 complement of the stomatogastric ganglion and brain in the adult and embryonic lobster,  
 1004 *Homarus americanus*. *Journal of neurochemistry* **105**:690–702.

1005 **Casanova B,** Brunet M, Segonzac M. 1993. Bacterian epibiosis impact on the morphology of shrimps  
 1006 associated with hydrothermalism in the Mid-Atlantic. *Cahiers de Biologie Marine* **34**:573–588.

1007 **Cathalot C,** Rouxel O, et al. 2018. Rapport de mission BICOSE2 - partie géochimie / Scientifique et  
 1008 Instrumentation.

1009 **Chaigneau J.** 1994. Les organes des sens autres que ceux de la vision. *Traité de Zoologie* **7**:345–410.

1010 **Chamberlain SC.** 2000. Vision in hydrothermal vent shrimp. *Philosophical Transactions of the Royal  
 1011 Society of London B: Biological Sciences* **355**:1151–1154. [doi:10.1098/rstb.2000.0657](https://doi.org/10.1098/rstb.2000.0657)

1012 **Charlou JL,** Donval JP, Douville E, Jean-Baptiste P, Radford-Knoery J, Fouquet Y, Dapoigny A,  
 1013 Stievenard M. 2000. Compared geochemical signatures and the evolution of Menez Gwen  
 1014 (37°50'N) and Lucky Strike (37°17'N) hydrothermal fluids, south of the Azores Triple Junction on  
 1015 the Mid-Atlantic Ridge. *Chemical Geology* **171**:49–75. [doi:10.1016/S0009-2541\(00\)00244-8](https://doi.org/10.1016/S0009-2541(00)00244-8)

1016 **Charlou JL,** Donval JP, Fouquet Y, Jean-Baptiste P, Holm N. 2002. Geochemistry of high H<sub>2</sub> and CH<sub>4</sub>  
 1017 vent fluids issuing from ultramafic rocks at the Rainbow hydrothermal field (36°14'N, MAR).  
 1018 *Chemical Geology* **191**:345–359. [doi:10.1016/S0009-2541\(02\)00134-1](https://doi.org/10.1016/S0009-2541(02)00134-1)

1019 **Charlou JL,** Donval JP, Konn C, Ondréas H, Fouquet Y, Jean-Baptiste P, Fourré E. 2010. High  
 1020 production and fluxes of H<sub>2</sub> and CH<sub>4</sub> and evidence of abiotic hydrocarbon synthesis by  
 1021 serpentinization in ultramafic-hosted hydrothermal systems on the Mid-Atlantic Ridge.  
 1022 *Geophysical Monograph Series* **188**:265–296. [doi:10.1029/2008GM000752](https://doi.org/10.1029/2008GM000752)

1023 **Charmantier-Daures M,** Segonzac M. 1998. Organ of Bellonci and sinus gland in three decapods from  
 1024 Atlantic hydrothermal vents: *Rimicaris Exoculata*, *Chorocaris Chacei*, and *Segonzacia*  
 1025 *Mesatlantica*. *Journal of Crustacean Biology* **18**:213–223. [doi:10.2307/1549315](https://doi.org/10.2307/1549315)

1026 **Chausson F,** Sanglier S, Leize E, Hagège A, Bridges CR, Sarradin P-M, Shillito B, Lallier FH, Zal F. 2004.  
 1027 Respiratory adaptations to the deep-sea hydrothermal vent environment: the case of *Segonzacia*

- 1028 *mesatlantica*, a crab from the Mid-Atlantic Ridge. *Micron*, XIIIth International Conference on  
1029 Invertebrate Dioxygen Binding Proteins **35**:31–41. doi:10.1016/j.micron.2003.10.010
- 1030 **Chaves da Silva PG**, Benton JL, Sandeman DC, Beltz BS. 2012. Adult Neurogenesis in the Crayfish  
1031 Brain: The Hematopoietic Anterior Proliferation Center Has Direct Access to the Brain and Stem  
1032 Cell Niche. *Stem Cells and Development* **22**:1027–1041. doi:10.1089/scd.2012.0583
- 1033 **Childress JJ**, Fisher CR. 1992. The biology of hydrothermal vent animals: physiology, biochemistry,  
1034 and autotrophic symbioses. *Oceanography and Marine Biology: An Annual Review* **30**:337–441.
- 1035 **Christie AE**. 2016. Expansion of the neuropeptidome of the globally invasive marine crab *Carcinus*  
1036 *maenas*. *General and comparative endocrinology* **235**:150–169.
- 1037 **Christie AE**, Stemmler EA, Dickinson PS. 2010. Crustacean neuropeptides. *Cellular and Molecular Life*  
1038 *Sciences* **67**:4135–4169.
- 1039 **Corbari L**, Zbinden M, Cambon-Bonavita M-A, Gaill F, Compère P. 2008. Bacterial symbionts and  
1040 mineral deposits in the branchial chamber of the hydrothermal vent shrimp *Rimicaris exoculata*:  
1041 relationship to moult cycle. *Aquatic Biology* **1**:225–238.
- 1042 **Cottin D**, Shillito B, Chertemps T, Thatje S, Léger N, Ravaux J. 2010. Comparison of heat-shock  
1043 responses between the hydrothermal vent shrimp *Rimicaris exoculata* and the related coastal  
1044 shrimp *Palaemonetes varians*. *Journal of Experimental Marine Biology and Ecology* **393**:9–16.  
1045 doi:10.1016/j.jembe.2010.06.008
- 1046 **Cronin TW**, Porter ML. 2008. Exceptional variation on a common theme: the evolution of crustacean  
1047 compound eyes. *Evolution: Education and Outreach* **1**:463.
- 1048 **Derby CD**, Thiel M. 2014. Nervous Systems and Control of Behavior. Oxford University Press.
- 1049 **Derby CD**, Weissburg MJ. 2014. The chemical senses and chemosensory ecology of crustaceans. In:  
1050 Derby CD, Thiel M (Eds.), Nervous Systems and Control of Behavior: Vol. 3. Natural History of  
1051 Crustacea. Oxford University Press, New York, pp. 263–292.
- 1052 **Derby CD**, Fortier JK, Harrison PJH, Cate HS. 2003. The peripheral and central antennular pathway of  
1053 the Caribbean stomatopod crustacean *Neogonodactylus oerstedii*. *Arthropod Structure &*  
1054 *Development* **32**:175–188. doi:10.1016/S1467-8039(03)00048-3
- 1055 **Desbruyères D**, Almeida A, Biscoito M, Comtet T, Khripounoff A, Bris NL, Sarradin PM, Segonzac M.  
1056 2000. A review of the distribution of hydrothermal vent communities along the northern Mid-  
1057 Atlantic Ridge: dispersal vs. environmental controls. *Hydrobiologia* **440**:201–216. doi:10.1007/978-  
1058 94-017-1982-7\_19
- 1059 **Desbruyères D**, Biscoito M, Caprais J-C, Colaço A, Comtet T, Crassous P, Fouquet Y, Khripounoff A, Le  
1060 Bris N, Olu K, Riso R, Sarradin P-M, Segonzac M, Vangriesheim A. 2001. Variations in deep-sea  
1061 hydrothermal vent communities on the Mid-Atlantic Ridge near the Azores plateau. *Deep Sea*  
1062 *Research Part I: Oceanographic Research Papers* **48**:1325–1346. doi:10.1016/S0967-  
1063 0637(00)00083-2
- 1064 **Dircksen H**, Skiebe P, Abel B, Agricola H, Buchner K, Muren JE, Nässel DR. 1999. Structure,  
1065 distribution, and biological activity of novel members of the allatostatin family in the crayfish  
1066 *Orconectes limosus*. *Peptides* **20**:695–712.
- 1067 **Duffy JE**, Thiel M, editors. 2007. Evolutionary Ecology of Social and Sexual Systems: Crustaceans as  
1068 Model Organisms. Oxford, New York: Oxford University Press.
- 1069 **Duve H**, Johnsen AH, Maestro J-L, Scott AG, Jaros PP, Thorpe A. 1997. Isolation and identification of  
1070 multiple neuropeptides of the allatostatin superfamily in the shore crab *Carcinus maenas*.  
1071 *European Journal of Biochemistry* **250**:727–734.
- 1072 **Duve H**, Johnsen AH, Scott AG, Thorpe A. 2002. Allatostatins of the tiger prawn, *Penaeus monodon*  
1073 (Crustacea: Penaeidea). *Peptides* **23**:1039–1051.
- 1074 **Elofsson R**, Hessler RR. 1990. Central nervous system of *Hutchinsoniella macracantha*  
1075 (Cephalocarida). *Journal of Crustacean Biology* **10**:423–439.
- 1076 **Fanenbruck M**, Harzsch S. 2005. A brain atlas of *Godzilliognomus frondosus* Yager, 1989 (Remipedia,  
1077 Godzilliidae) and comparison with the brain of *Speleonectes tulumensis* Yager, 1987 (Remipedia,  
1078 Speleonectidae): implications for arthropod relationships. *Arthropod Structure & Development*,  
1079 Arthropod Brain Morphology and Evolution **34**:343–378. doi:10.1016/j.asd.2005.01.007

1080 **Fanenbruck M**, Harzsch S, Wägele JW. 2004. The brain of the Remipedia (Crustacea) and an  
1081 alternative hypothesis on their phylogenetic relationships. *Proceedings of the National Academy*  
1082 *of Sciences* **101**:3868–3873. doi:10.1073/pnas.0306212101

1083 **Fisher CR**, Takai K, Le Bris N. 2007. Hydrothermal Vent Ecosystems. *Oceanography* **20**:14–23.

1084 **Fontaine MT**, Passelecq-Gerin E, Bauchau AG. 1982. Structures chemoreceptrices des antennules du  
1085 crabe *Carcinus Maenas* (L.) (Decapoda Brachyura). *Crustaceana* **43**:271–283.  
1086 doi:10.1163/156854082X00218

1087 **Garm A**, Hallberg E, Høeg JT. 2003. Role of maxilla 2 and its setae during feeding in the shrimp  
1088 *Palaemon adspersus* (Crustacea: Decapoda). *The Biological Bulletin* **204**:126–137.  
1089 doi:10.2307/1543548

1090 **Garm A**, Shabani S, Høeg JT, Derby CD. 2005. Chemosensory neurons in the mouthparts of the spiny  
1091 lobsters *Panulirus argus* and *Panulirus interruptus* (Crustacea: Decapoda). *Journal of Experimental*  
1092 *Marine Biology and Ecology* **314**:175–186. doi:10.1016/j.jembe.2004.08.016

1093 **Garm A**, Watling L. 2013. The crustacean integument: setae, setules, and other ornamentation.  
1094 *Functional Morphology and Diversity* **1**:167–198.

1095 **Gaten E**, Herring PJ, Shelton PA. 1998. The development and evolution of the eyes of vent shrimps  
1096 (Decapoda: Bresiliidae). *Cahiers de Biologie Marine* **39**:287–290.

1097 **Gebruk AV**, Galkin SV, Vereshchaka AL, Moskalev LI, Southward AJ. 1997. Ecology and biogeography  
1098 of the hydrothermal vent fauna of the Mid-Atlantic Ridge. In: Blaxter JHS, Southward AJ, Gebruk  
1099 AV, Southward EC, Tyler PA (Eds.), *Advances in Marine Biology, The Biogeography of the Oceans*.  
1100 Academic Press. pp. 93–144. doi:10.1016/S0065-2881(08)60016-4

1101 **Grünert U**, Ache BW. 1988. Ultrastructure of the aesthetasc (olfactory) sensilla of the spiny lobster,  
1102 *Panulirus argus*. *Cell Tissue Res* **251**:95–103. doi:10.1007/BF00215452

1103 **Guenther CM**, Atema J. 1998. Distribution of setae on the *Homarus americanus* lateral antennular  
1104 flagellum. *The Biological Bulletin* **195**:182–183. doi:10.2307/1542827

1105 **Hallberg E**, Skog M. 2011. Chemosensory sensilla in crustaceans. In: Breithaupt T, Thiel M (Eds.),  
1106 *Chemical Communication in Crustaceans*. Springer, New York, pp. 103–121.

1107 **Harzsch S**. 2002. The phylogenetic significance of crustacean optic neuropils and chiasmata: a re-  
1108 examination. *Journal of Comparative Neurology* **453**:10–21.

1109 **Harzsch S**, Anger K, Dawirs RR. 2002. Immunocytochemical detection of acetylated alpha-tubulin and  
1110 *Drosophila* synapsin in the embryonic crustacean nervous system. *International Journal of*  
1111 *Developmental Biology* **41**:477–484.

1112 **Harzsch S**, Benton J, Dawirs RR, Beltz B. 1999. A new look at embryonic development of the visual  
1113 system in decapod crustaceans: neuropil formation, neurogenesis, and apoptotic cell death.  
1114 *Journal of neurobiology* **39**:294.

1115 **Harzsch S**, Hansson BS. 2008. Brain architecture in the terrestrial hermit crab *Coenobita clypeatus*  
1116 (Anomura, Coenobitidae), a crustacean with a good aerial sense of smell. *BMC Neuroscience* **9**:58.  
1117 doi:10.1186/1471-2202-9-58

1118 **Harzsch S**, Krieger J. 2018. Crustacean olfactory systems: A comparative review and a crustacean  
1119 perspective on olfaction in insects. *Progress in Neurobiology* **161**:23–60.  
1120 doi:10.1016/j.pneurobio.2017.11.005

1121 **Harzsch S**, Miller J, Benton J, Dawirs RR, Beltz B. 1998. Neurogenesis in the thoracic neuromeres of  
1122 two crustaceans with different types of metamorphic development. *Journal of Experimental*  
1123 *Biology* **201**:2465–2479.

1124 **Harzsch S**, Rieger V, Krieger J, Seefluth F, Strausfeld NJ, Hansson BS. 2011. Transition from marine to  
1125 terrestrial ecologies: changes in olfactory and tritocerebral neuropils in land-living isopods.  
1126 *Arthropod structure & development* **40**:244–257.

1127 **Herring PJ**, Gaten E, Shelton PMJ. 1999. Are vent shrimps blinded by science? *Nature* **398**:116.  
1128 doi:10.1038/18142

1129 **Hourdez S**, Lallier FH. 2006. Adaptations to hypoxia in hydrothermal-vent and cold-seep  
1130 invertebrates. In: *Life in Extreme Environments*. Springer. pp. 297–313.

- 1131 **Hügler M**, Petersen JM, Dubilier N, Imhoff JF, Sievert SM. 2011. Pathways of carbon and energy  
1132 metabolism of the epibiotic community associated with the deep-sea hydrothermal vent shrimp  
1133 *Rimicaris exoculata*. *PLoS One* **6**:e16018.
- 1134 **Huybrechts J**, Nusbaum MP, Bosch LV, Baggerman G, De Loof A, Schoofs L. 2003. Neuropeptidomic  
1135 analysis of the brain and thoracic ganglion from the Jonah crab, *Cancer borealis*. *Biochemical and*  
1136 *biophysical research communications* **308**:535–544.
- 1137 **Jannasch HW**, Mottl MJ. 1985. Geomicrobiology of deep-sea hydrothermal vents. *Science* **229**:717–  
1138 725. doi:10.1126/science.229.4715.717
- 1139 **Jinks RN**, Battelle B-A, Herzog ED, Kass L, Renninger GH, Chamberlain SC. 1998. Sensory adaptations  
1140 in hydrothermal vent shrimps from the Mid-Atlantic Ridge. *Cahiers de Biologie Marine* **39**:309–  
1141 312.
- 1142 **Johnson KS**, Beehler CL, Sakamoto-Arnold CM, Childress JJ. 1986. *In situ* measurements of chemical  
1143 distributions in a deep-sea hydrothermal vent field. *Science* **231**:1139–1141.  
1144 doi:10.1126/science.231.4742.1139
- 1145 **Johnson KS**, Childress JJ, Beehler CL. 1988. Short-term temperature variability in the Rose Garden  
1146 hydrothermal vent field: an unstable deep-sea environment. *Deep Sea Research Part A*  
1147 *Oceanographic Research Papers* **35**:1711–1721. doi:10.1016/0198-0149(88)90045-3
- 1148 **Johnson ML**, Shelton PMJ, Herring PJ, Gardner S. 1995. Spectral responses from the dorsal organ of a  
1149 juvenile *Rimicaris exoculata* from the TAG hydrothermal vent site. *BRIDGE Newsletter* **8**:38–42.
- 1150 **Jr DFM**, Alones VE. 1997. Response properties of higher level neurons in the central olfactory  
1151 pathway of the crayfish. *Journal of Comparative Physiology A* **181**:205–216.  
1152 doi:10.1007/s003590050107
- 1153 **Kenning M**, Harzsch S. 2013. Brain anatomy of the marine isopod *Saduria entomon* Linnaeus, 1758  
1154 (Valvifera, Isopoda) with special emphasis on the olfactory pathway. *Frontiers in neuroanatomy*  
1155 **7**:32.
- 1156 **Kenning M**, Müller C, Wirkner CS, Harzsch S. 2013. The Malacostraca (Crustacea) from a  
1157 neurophylogenetic perspective: New insights from brain architecture in *Nebalia herbstii* Leach,  
1158 1814 (Leptostraca, Phyllocarida). *Zoologischer Anzeiger - A Journal of Comparative Zoology*  
1159 **252**:319–336. doi:10.1016/j.jcz.2012.09.003
- 1160 **Klages BR**, Heimbeck G, Godenschwege TA, Hofbauer A, Pflugfelder GO, Reifegerste R, Reisch D,  
1161 Schaupp M, Buchner S, Buchner E. 1996. Invertebrate synapsins: a single gene codes for several  
1162 isoforms in *Drosophila*. *Journal of Neuroscience* **16**:3154–3165.
- 1163 **Klaus S**, Mendoza JC, Liew JH, Plath M, Meier R, Yeo DC. 2013. Rapid evolution of troglomorphic  
1164 characters suggests selection rather than neutral mutation as a driver of eye reduction in cave  
1165 crabs. *Biology letters* **9**:20121098.
- 1166 **Kreissl S**, Strasser C, Galizia CG. 2010. Allatostatin immunoreactivity in the honeybee brain. *Journal of*  
1167 *Comparative Neurology* **518**:1391–1417.
- 1168 **Krieger J**, Braun P, Rivera NT, Schubart CD, Müller CHG, Harzsch S. 2015. Comparative analyses of  
1169 olfactory systems in terrestrial crabs (Brachyura): evidence for aerial olfaction? *PeerJ* **3**:e1433.  
1170 doi:10.7717/peerj.1433
- 1171 **Krieger J**, Grandy R, Drew MM, Erland S, Stensmyr MC, Harzsch S, Hansson BS. 2012a. Giant Robber  
1172 Crabs Monitored from Space: GPS-Based Telemetric Studies on Christmas Island (Indian Ocean).  
1173 *PLOS ONE* **7**:e49809. doi:10.1371/journal.pone.0049809
- 1174 **Krieger J**, Sandeman RE, Sandeman DC, Hansson BS, Harzsch S. 2010. Brain architecture of the largest  
1175 living land arthropod, the Giant Robber Crab *Birgus latro* (Crustacea, Anomura, Coenobitidae):  
1176 evidence for a prominent central olfactory pathway? *Frontiers in Zoology* **7**:25. doi:10.1186/1742-  
1177 9994-7-25
- 1178 **Krieger J**, Sombke A, Seefluth F, Kenning M, Hansson BS, Harzsch S. 2012b. Comparative brain  
1179 architecture of the European shore crab *Carcinus maenas* (Brachyura) and the common hermit  
1180 crab *Pagurus bernhardus* (Anomura) with notes on other marine hermit crabs. *Cell and Tissue*  
1181 *Research* **348**:47–69. doi:10.1007/s00441-012-1353-4

1182 **Lallier FH**, Truchot J-P. 1997. Hemocyanin oxygen-binding properties of a deep-sea hydrothermal  
1183 vent shrimp: Evidence for a novel cofactor. *Journal of Experimental Zoology* **277**:357–364.  
1184 [doi:10.1002/\(SICI\)1097-010X\(19970401\)277:5<357::AID-JEZ1>3.0.CO;2-O](https://doi.org/10.1002/(SICI)1097-010X(19970401)277:5<357::AID-JEZ1>3.0.CO;2-O)

1185 **Le Bris N**, Zbinden M, Gaill F. 2005. Processes controlling the physico-chemical micro-environments  
1186 associated with Pompeii worms. *Deep Sea Research Part I: Oceanographic Research Papers*  
1187 **52**:1071–1083. [doi:10.1016/j.dsr.2005.01.003](https://doi.org/10.1016/j.dsr.2005.01.003)

1188 **Loesel R**, Wolf H, Kenning M, Harzsch S, Sombke A. 2013. Architectural principles and evolution of  
1189 the Arthropod central nervous system. In: Minelli A, Boxhsall G, Fusco G (Eds.), *Arthropod Biology*  
1190 *and Evolution*. Berlin, Heidelberg, pp. 299–342. [doi:10.1007/978-3-642-36160-9\\_13](https://doi.org/10.1007/978-3-642-36160-9_13)

1191 **Lunina AA**, Vereshchaka AL. 2014. Distribution of hydrothermal alvinocaridid shrimps: effect of  
1192 geomorphology and specialization to extreme biotopes. *PLoS one* **9**:e92802.

1193 **Luther III GW**, Rozan TF, Taillefert M, Nuzzio DB, Di Meo C, Shank TM, Lutz RA, Cary SC. 2001.  
1194 Chemical speciation drives hydrothermal vent ecology. *Nature* **410**:813.

1195 **Ma M**, Gard AL, Xiang F, Wang J, Davoodian N, Lenz PH, Malecha SR, Christie AE, Li L. 2010.  
1196 Combining in silico transcriptome mining and biological mass spectrometry for neuropeptide  
1197 discovery in the Pacific white shrimp *Litopenaeus vannamei*. *Peptides* **31**:27–43.

1198 **Machon J**, Lucas P, Ravaux J, Zbinden M. 2018. Comparison of chemoreceptive abilities of the  
1199 hydrothermal shrimp *Mirocaris fortunata* and the coastal shrimp *Palaemon elegans*. *Chemical*  
1200 *senses* **43**(7):489–501. [doi:https://doi.org/10.1093/chemse/bjy041](https://doi.org/10.1093/chemse/bjy041)

1201 **Maza FJ**, Sztarker J, Shkedy A, Peszano VN, Locatelli FF, Delorenzi A. 2016. Context-dependent  
1202 memory traces in the crab's mushroom bodies: Functional support for a common origin of high-  
1203 order memory centers. *PNAS* **113**:E7957–E7965. [doi:10.1073/pnas.1612418113](https://doi.org/10.1073/pnas.1612418113)

1204 **McGaw IJ**. 2005. The decapod crustacean circulatory system: A case that is neither open nor closed.  
1205 *Microscopy and Microanalysis* **11**:18–36. [doi:10.1017/S1431927605050026](https://doi.org/10.1017/S1431927605050026)

1206 **McGaw IJ**, Reiber CL. 2002. Cardiovascular system of the blue crab *Callinectes sapidus*. *Journal of*  
1207 *Morphology* **251**:1–21. [doi:10.1002/jmor.1071](https://doi.org/10.1002/jmor.1071)

1208 **McKinzie ME**, Benton JL, Beltz BS, Mellon D. 2003. Parasol cells of the hemiellipsoid body in the  
1209 crayfish *Procambarus clarkii*: Dendritic branching patterns and functional implications. *Journal of*  
1210 *Comparative Neurology* **462**:168–179. [doi:10.1002/cne.10716](https://doi.org/10.1002/cne.10716)

1211 **McMahon BR**. 2001. Control of cardiovascular function and its evolution in Crustacea. *Journal of*  
1212 *Experimental Biology* **204**:923–932.

1213 **Mellon D**. 2014. Sensory systems of crustaceans. In: Derby C, Thiel M, Thiel M (Eds.), *The Natural*  
1214 *History of the Crustacea* **3**:49–84.

1215 **Mellon D**. 2012. Smelling, feeling, tasting and touching: behavioral and neural integration of  
1216 antennular chemosensory and mechanosensory inputs in the crayfish. *Journal of Experimental*  
1217 *Biology* **215**:2163–2172. [doi:10.1242/jeb.069492](https://doi.org/10.1242/jeb.069492)

1218 **Mellon D**. 2003. Dendritic initiation and propagation of spikes and spike bursts in a multimodal  
1219 sensory interneuron: The crustacean parasol cell. *Journal of Neurophysiology* **90**:2465–2477.  
1220 [doi:10.1152/jn.00310.2003](https://doi.org/10.1152/jn.00310.2003)

1221 **Mellon D**. 2000. Convergence of multimodal sensory input onto higher-level neurons of the crayfish  
1222 olfactory pathway. *Journal of Neurophysiology* **84**:3043–3055. [doi:10.1152/jn.2000.84.6.3043](https://doi.org/10.1152/jn.2000.84.6.3043)

1223 **Mellon D**, Sandeman DC, Sandeman RE. 1992. Characterization of oscillatory olfactory interneurons  
1224 in the protocerebrum of the crayfish. *Journal of Experimental Biology* **167**:15–38.

1225 **Mellon D**, Wheeler CJ. 1999. Coherent oscillations in membrane potential synchronize impulse bursts  
1226 in central olfactory neurons of the crayfish. *Journal of Neurophysiology* **81**:1231–1241.  
1227 [doi:10.1152/jn.1999.81.3.1231](https://doi.org/10.1152/jn.1999.81.3.1231)

1228 **Mellon D**, Alones V, Lawrence MD. 1992. Anatomy and fine structure of neurons in the  
1229 deutocerebral projection pathway of the crayfish olfactory system. *Journal of Comparative*  
1230 *Neurology* **321**:93–111. [doi:10.1002/cne.903210109](https://doi.org/10.1002/cne.903210109)

1231 **Meth R**, Wittfoth C, Harzsch S. 2017. Brain architecture of the Pacific White Shrimp *Penaeus*  
1232 *vannamei* Boone, 1931 (Malacostraca, Dendrobranchiata): correspondence of brain structure and  
1233 sensory input? *Cell and Tissue Research* **369**:255–271. [doi:10.1007/s00441-017-2607-y](https://doi.org/10.1007/s00441-017-2607-y)

1234 **Moran D**, Softley R, Warrant EJ. 2015. The energetic cost of vision and the evolution of eyeless  
1235 Mexican cavefish. *Science advances* **1**:e1500363.

1236 **Nässel DR**, Homberg U. 2006. Neuropeptides in interneurons of the insect brain. *Cell and Tissue*  
1237 *Research* **326**:1.

1238 **Niven JE**, Laughlin SB. 2008. Energy limitation as a selective pressure on the evolution of sensory  
1239 systems. *Journal of Experimental Biology* **211**:1792–1804. doi:10.1242/jeb.017574

1240 **Nuckley DJ**, Jinks RN, Battelle BA, Herzog ED, Kass L, Renninger GH, Chamberlain SC. 1996. Retinal  
1241 anatomy of a new species of bresiliid shrimp from a hydrothermal vent field on the Mid-Atlantic  
1242 Ridge. *The Biological Bulletin* **190**:98–110. doi:10.2307/1542679

1243 **O'Neill PJ**, Jinks RN, Herzog ED, Battelle B-A, Kass L, Renninger GH, Chamberlain SC. 1995. The  
1244 morphology of the dorsal eye of the hydrothermal vent shrimp, *Rimicaris exoculata*. *Visual*  
1245 *Neuroscience* **12**:861–875. doi:10.1017/S0952523800009421

1246 **Pelli DG**, Chamberlain SC. 1989. The visibility of 350 °C black-body radiation by the shrimp *Rimicaris*  
1247 *exoculata* and man. *Nature* **337**:460–461. doi:10.1038/337460a0

1248 **Petersen JM**, Ramette A, Lott C, Cambon-Bonavita M-A, Zbinden M, Dubilier N. 2010. Dual symbiosis  
1249 of the vent shrimp *Rimicaris exoculata* with filamentous gamma- and epsilonproteobacteria at  
1250 four Mid-Atlantic Ridge hydrothermal vent fields. *Environmental Microbiology* **12**:2204–2218.  
1251 doi:10.1111/j.1462-2920.2009.02129.x

1252 **Polanska MA**, Tuchina O, Agricola H, Hansson BS, Harzsch S. 2012. Neuropeptide complexity in the  
1253 crustacean central olfactory pathway: immunolocalization of A-type allatostatins and RFamide-  
1254 like peptides in the brain of a terrestrial hermit crab. *Molecular Brain* **5**:29. doi:10.1186/1756-  
1255 6606-5-29

1256 **Polanska MA**, Yasuda A, Harzsch S. 2007. Immunolocalisation of crustacean-SIFamide in the median  
1257 brain and eyestalk neuropils of the marbled crayfish. *Cell and Tissue Research* **330**:331–344.

1258 **Ponsard J**, Cambon-Bonavita M-A, Zbinden M, Lepoint G, Joassin A, Corbari L, Shillito B, Durand L,  
1259 Cueff-Gauchard V, Compère P. 2013. Inorganic carbon fixation by chemosynthetic ectosymbionts  
1260 and nutritional transfers to the hydrothermal vent host-shrimp *Rimicaris exoculata*. *The ISME*  
1261 *Journal* **7**:96–109. doi:10.1038/ismej.2012.87

1262 **Pynnönen K**. 1985. The structure of long distance (antennular) chemoreceptors in *Saduria entomon*  
1263 (L.), Isopoda, and their role in feeding behaviour. *Annales Zoologici Fennici* **22**:423–432.

1264 **Ramm T**, Scholtz G. 2017. No sight, no smell? – Brain anatomy of two amphipod crustaceans with  
1265 different lifestyles. *Arthropod Structure & Development* **46**:537–551.  
1266 doi:10.1016/j.asd.2017.03.003

1267 **Rathke MH**. 1837. Bertrag zur fauna der krym. *Mémoires de l'Académie Impériale des Sciences de St*  
1268 *Petersbourg* **3**:371–380.

1269 **Ravaux J**, Gaill F, Bris NL, Sarradin P-M, Jollivet D, Shillito B. 2003. Heat-shock response and  
1270 temperature resistance in the deep-sea vent shrimp *Rimicaris exoculata*. *Journal of Experimental*  
1271 *Biology* **206**:2345–2354. doi:10.1242/jeb.00419

1272 **Reiber CL**, McMahon BR. 1998. The effects of progressive hypoxia on the crustacean cardiovascular  
1273 system: a comparison of the freshwater crayfish, (*Procambarus clarkii*), and the lobster (*Homarus*  
1274 *americanus*). *Journal of Comparative Physiology B* **168**:168–176. doi:10.1007/s003600050133

1275 **Renninger GH**, Kass L, Gleeson RA, Van Dover CL, Battelle B-A, Jinks RN, Herzog ED, Chamberlain SC.  
1276 1995. Sulfide as a chemical stimulus for deep-sea hydrothermal vent shrimp. *The Biological*  
1277 *Bulletin* **189**:69–76. doi:10.2307/1542456

1278 **Reynolds GT**, Lutz RA. 2001. Sources of light in the deep ocean. *Reviews of Geophysics* **39**:123–136.

1279 **Richter S**, Loesel R, Purschke G, Schmidt-Rhaesa A, Scholtz G, Stach T, Vogt L, Wanninger A, Brenneis  
1280 G, Döring C. 2010. Invertebrate neurophylogeny: suggested terms and definitions for a  
1281 neuroanatomical glossary. *Frontiers in Zoology* **7**:29.

1282 **Richter S**, Scholtz G. 2001. Phylogenetic analysis of the Malacostraca (Crustacea). *Journal of*  
1283 *Zoological Systematics and Evolutionary Research* **39**:113–136. doi:10.1046/j.1439-  
1284 0469.2001.00164.x

- 1285 **Rona PA**, Klinkhammer G, Nelsen TA, Trefry JH, Elderfield H. 1986. Black smokers, massive sulphides  
1286 and vent biota at the Mid-Atlantic Ridge. *Nature* **321**:33.
- 1287 **Sandeman D**, Callan Harold Garnet. 1967. The vascular circulation in the brain, optic lobes and  
1288 thoracic ganglia of the crab *Carcinus*. *Proceedings of the Royal Society of London Series B*  
1289 *Biological Sciences* **168**:82–90. doi:10.1098/rspb.1967.0052
- 1290 **Sandeman D**, Kenning M, Harzsch S. 2014a. Adaptive trends in malacostracan brain form and  
1291 function related to behavior. *Crustacean Nervous System and Their Control of Behaviour, The*  
1292 *Natural History of the Crustacea* **3**:11–48.
- 1293 **Sandeman D**, Kenning M, Harzsch S. 2014b. Adaptive trends in malacostracan brain form and  
1294 function related to behavior. In: Derby C, Thiel M (Eds.), *Crustacean Nervous System and Their*  
1295 *Control of Behavior*, Vol. 3. Oxford University Press, New York, pp. 11–48.
- 1296 **Sandeman D**, Sandeman R, Derby C, Schmidt M. 1992. Morphology of the Brain of Crayfish, Crabs,  
1297 and Spiny Lobsters: A Common Nomenclature for Homologous Structures. *The Biological Bulletin*  
1298 **183**:304–326. doi:10.2307/1542217
- 1299 **Sandeman D**, Scholtz G, Sandeman RE. 1993. Brain evolution in decapod crustacea. *Journal of*  
1300 *Experimental Zoology* **265**:112–133. doi:10.1002/jez.1402650204
- 1301 **Sanders NK**, Arp AJ, Childress JJ. 1988. Oxygen binding characteristics of the hemocyanins of two  
1302 deep-sea hydrothermal vent crustaceans. *Respiration Physiology* **71**:57–67. doi:10.1016/0034-  
1303 5687(88)90115-6
- 1304 **Schachtner J**, Schmidt M, Homberg U. 2005. Organization and evolutionary trends of primary  
1305 olfactory brain centers in Tetraconata (Crustacea+Hexapoda). *Arthropod Structure &*  
1306 *Development, Arthropod Brain Morphology and Evolution* **34**:257–299.  
1307 doi:10.1016/j.asd.2005.04.003
- 1308 **Schmidt C**, Le Bris N, Gaill F. 2008. Interactions of deep-sea vent invertebrates with their  
1309 environment: The case of *Rimicaris exoculata*. *Journal of Shellfish Research* **27**:79–90.  
1310 doi:10.2983/0730-8000(2008)27[79:IODVIW]2.0.CO;2
- 1311 **Schmidt M**. 2016. Malacostraca. In: Schmidt-Rhaesa A, Harzsch S, Purschke G (Eds.), *Structure &*  
1312 *Evolution of Invertebrate Nervous Systems*. Oxford University Press, Oxford, pp. 529–582.
- 1313 **Schmidt M**, Ache BW. 1997. Immunocytochemical analysis of glomerular regionalization and  
1314 neuronal diversity in the olfactory deutocerebrum of the spiny lobster. *Cell and Tissue Research*  
1315 **287**:541–563. doi:10.1007/s004410050778
- 1316 **Schmidt M**, Gnatzy W. 1984. Are the funnel-canal organs the ‘campaniform sensilla’ of the shore  
1317 crab, *Carcinus maenas* (Decapoda, Crustacea)? *Cell and Tissue Research* **237**:81–93.  
1318 doi:10.1007/BF00229202
- 1319 **Schmidt M**, Mellon D. 2010. Neuronal processing of chemical information in crustaceans. In:  
1320 Breithaupt T, Thiel M (Eds.), *Chemical Communication in Crustaceans*. Springer, New York, pp.  
1321 123–147. doi:10.1007/978-0-387-77101-4\_7
- 1322 **Scholtz G**, Richter S. 1995. Phylogenetic systematics of the reptantian Decapoda (Crustacea,  
1323 Malacostraca). *Zoological Journal of the Linnean Society* **113**:289–328.
- 1324 **Scholz S**, Richter S, Wirkner CS. 2018. Constant morphological patterns in the hemolymph vascular  
1325 system of crayfish (Crustacea, Decapoda). *Arthropod Structure & Development* **47**:248–267.  
1326 doi:10.1016/j.asd.2017.12.005
- 1327 **Segonzac M**, De Saint Laurent M, Casanova B. 1993. L’énigme du comportement trophique des  
1328 crevettes Alvinocarididae des sites hydrothermaux de la dorsale médio-atlantique. *Cahiers De*  
1329 *Biologie Marine* **34**:535–571.
- 1330 **Shillito B**, Hamel G, Duchi C, Cottin D, Sarrazin J, Sarradin P-M, Ravaux J, Gaill F. 2008. Live capture of  
1331 megafauna from 2300m depth, using a newly designed Pressurized Recovery Device. *Deep Sea*  
1332 *Research Part I: Oceanographic Research Papers* **55**:881–889. doi:10.1016/j.dsr.2008.03.010
- 1333 **Sinakevitch I**, Douglass JK, Scholtz G, Loesel R, Strausfeld NJ. 2003. Conserved and convergent  
1334 organization in the optic lobes of insects and isopods, with reference to other crustacean taxa.  
1335 *Journal of Comparative Neurology* **467**:150–172.

- 1336 **Sitaraman D**, Zars M, LaFerriere H, Chen Y-C, Sable-Smith A, Kitamoto T, Rottinghaus GE, Zars T.  
1337 2008. Serotonin is necessary for place memory in *Drosophila*. *Proceedings of the National*  
1338 *Academy of Sciences* **105**:5579–5584.
- 1339 **Sombke A**, Lipke E, Michalik P, Uhl G, Harzsch S. 2015. Potential and limitations of X-Ray micro-  
1340 computed tomography in arthropod neuroanatomy: A methodological and comparative survey.  
1341 *Journal of Comparative Neurology* **523**:1281–1295.
- 1342 **Stay B**, Tobe SS. 2007. The role of allatostatins in juvenile hormone synthesis in insects and  
1343 crustaceans. *Annual Review of Entomology* **52**:277–299.
- 1344 **Stay B**, Tobe SS, Bendena WG. 1995. Allatostatins: identification, primary structures, functions and  
1345 distribution. *Advances in Insect Physiology* **25**:267–337.
- 1346 **Stegner ME**, Richter S. 2011. Morphology of the brain in *Hutchinsoniella macracantha*  
1347 (Cephalocarida, Crustacea). *Arthropod structure & development* **40**:221–243.
- 1348 **Stegner ME**, Stemme T, Iliffe TM, Richter S, Wirkner CS. 2015. The brain in three crustaceans from  
1349 cavernous darkness. *BMC Neuroscience* **16**:19. doi:10.1186/s12868-015-0138-6
- 1350 **Steinacker A**. 1979. Neural and neurosecretory control of the decapod crustacean auxiliary heart.  
1351 *Integrative and Comparative Biology* **19**:67–75. doi:10.1093/icb/19.1.67
- 1352 **Steinacker A**. 1978. The anatomy of the decapod crustacean auxiliary heart. *The Biological Bulletin*  
1353 **154**:497–507. doi:10.2307/1541075
- 1354 **Stemme T**, Eickhoff R, Bicker G. 2014. Olfactory projection neuron pathways in two species of marine  
1355 Isopoda (Peracarida, Malacostraca, Crustacea). *Tissue and Cell* **46**:260–263.
- 1356 **Stemme T**, Harzsch S. 2016. Remipedia. In: Schmidt-Rhaesa A, Harzsch S, Günter P (Eds.), Structure  
1357 and evolution of invertebrate nervous systems. Oxford University Press, pp 522–528.
- 1358 **Strausfeld NJ**. 2012. Arthropod Brains: Evolution, Functional Elegance, and Historical Significance.  
1359 Cambridge, Mass: Belknap Press.
- 1360 **Strausfeld NJ**. 2009. Brain organization and the origin of insects: an assessment. *Proceedings of the*  
1361 *Royal Society B: Biological Sciences* **276**:1929–1937. doi:10.1098/rspb.2008.1471
- 1362 **Strausfeld NJ**. 2005. The evolution of crustacean and insect optic lobes and the origins of chiasmata.  
1363 *Arthropod Structure & Development* **34**:235–256.
- 1364 **Strausfeld NJ**. 1998. Crustacean – Insect relationships: The use of brain characters to derive  
1365 phylogeny amongst segmented invertebrates. *Brain Behavior and Evolution* **52**:186–206.  
1366 doi:10.1159/000006563
- 1367 **Strausfeld NJ**, Nassel DR. 1981. Neuroarchitectures serving compound eyes of Crustacea and insects.  
1368 *Handbook of sensory physiology*.
- 1369 **Sullivan JM**, Beltz BS. 2005. Integration and segregation of inputs to higher-order neuropils of the  
1370 crayfish brain. *Journal of Comparative Neurology* **481**:118–126. doi:10.1002/cne.20346
- 1371 **Sullivan JM**, Beltz BS. 2004. Evolutionary changes in the olfactory projection neuron pathways of  
1372 eumalacostracan crustaceans. *Journal of Comparative Neurology* **470**:25–38.  
1373 doi:10.1002/cne.11026
- 1374 **Sullivan JM**, Beltz BS. 2001. Neural pathways connecting the deutocerebrum and lateral  
1375 protocerebrum in the brains of decapod crustaceans. *Journal of Comparative Neurology* **441**:9–  
1376 22. doi:10.1002/cne.1394
- 1377 **Sullivan JM**, Benton JL, Sandeman DC, Beltz BS. 2007. Adult neurogenesis: a common strategy across  
1378 diverse species. *Journal of Comparative Neurology* **500**:574–584.
- 1379 **Sztarker J**, Strausfeld N, Andrew D, Tomsic D. 2009. Neural organization of first optic neuropils in the  
1380 littoral crab *Hemigrapsus oregonensis* and the semiterrestrial species *Chasmagnathus granulatus*.  
1381 *Journal of Comparative Neurology* **513**:129–150.
- 1382 **Sztarker J**, Strausfeld NJ, Tomsic D. 2005. Organization of optic lobes that support motion detection  
1383 in a semiterrestrial crab. *Journal of Comparative Neurology* **493**:396–411.
- 1384 **Tapley DW**, Buettner GR, Shick JM. 1999. Free radicals and chemiluminescence as products of the  
1385 spontaneous oxidation of sulfide in seawater, and their biological implications. *The Biological*  
1386 *Bulletin* **196**:52–56.
- 1387 **Thiel M**, Breithaupt T. 2011. Chemical Communication in Crustaceans. Springer, New York.

- 1388 **Thiel M**, Watling L, editors. 2015. Lifestyles and Feeding Biology, Natural History of Crustacea.  
1389 Oxford, New York: Oxford University Press.
- 1390 **Tuchina O**, Koczan S, Harzsch S, Rybak J, Wolff G, Strausfeld NJ, Hansson BS. 2015. Central  
1391 projections of antennular chemosensory and mechanosensory afferents in the brain of the  
1392 terrestrial hermit crab (*Coenobita clypeatus*; Coenobitidae, Anomura). *Front Neuroanat* **9**:94.  
1393 doi:10.3389/fnana.2015.00094
- 1394 **Van Dover CL**. 2000. The ecology of deep-sea hydrothermal vents. Princeton University Press.
- 1395 **Van Dover CL**, Fry B. 1994. Microorganisms as food resources at deep-sea hydrothermal vents.  
1396 *Limnology and Oceanography* **39**:51–57.
- 1397 **Van Dover CL**, Fry B, Grassle JF, Humphris S, Rona PA. 1988. Feeding biology of the shrimp *Rimicaris*  
1398 *exoculata* at hydrothermal vents on the Mid-Atlantic Ridge. *Marine Biology* **98**:209–216.  
1399 doi:10.1007/BF00391196
- 1400 **Van Dover CL**, Reynolds GT, Chave AD, Tyson JA. 1996. Light at deep-sea hydrothermal vents.  
1401 *Geophysical research letters* **23**:2049–2052.
- 1402 **Van Dover CL**, Szuts EZ, Chamberlain SC, Cann JR. 1989. A novel eye in “eyeless” shrimp from  
1403 hydrothermal vents of the Mid-Atlantic Ridge. *Nature* **337**:458–460. doi:10.1038/337458a0
- 1404 **Vitzthum H**, Homberg U, Agricola H. 1996. Distribution of Dip-allatostatin I-like immunoreactivity in  
1405 the brain of the locust *Schistocerca gregaria* with detailed analysis of immunostaining in the  
1406 central complex. *Journal of Comparative Neurology* **369**:419–437.
- 1407 **Welsch U**, Mulisch M. 2010. Romeis Mikroskopische Technik. *Springer Spektrum* **551**:03728–14.
- 1408 **White SN**. 2000. An investigation into the characteristics and sources of light emission at deep-sea  
1409 hydrothermal vents. doi:10.1575/1912/4053
- 1410 **White SN**, Chave AD, Reynolds GT, Van Dover CL. 2002. Ambient light emission from hydrothermal  
1411 vents on the Mid-Atlantic Ridge. *Geophysical research letters* **29**.
- 1412 **Wilkens JL**. 1999. Evolution of the cardiovascular system in Crustacea. *Integrative and Comparative*  
1413 *Biology* **39**:199–214. doi:10.1093/icb/39.2.199
- 1414 **Williams AB**, Rona PA. 1986. Two new caridean shrimps (Bresiliidae) from a hydrothermal field on  
1415 the Mid-Atlantic Ridge. *Journal of Crustacean Biology* **6**:446–462. doi:10.2307/1548184
- 1416 **Wirkner CS**, Richter S. 2010. Evolutionary morphology of the circulatory system in Peracarida  
1417 (Malacostraca; Crustacea). *Cladistics* **26**:143–167. doi:10.1111/j.1096-0031.2009.00278.x
- 1418 **Wittfoth C**, Harzsch S. 2018. Adult neurogenesis in the central olfactory pathway of  
1419 dendrobranchiate and caridean shrimps: New insights into the evolution of the deutocerebral  
1420 proliferative system in reptant decapods. *Developmental Neurobiology* **78**:757–774.  
1421 doi:10.1002/dneu.22596
- 1422 **Wolff GH**, Harzsch S, Hansson BS, Brown S, Strausfeld N. 2012. Neuronal organization of the  
1423 hemiellipsoid body of the land hermit crab, *Coenobita clypeatus*: Correspondence with the  
1424 mushroom body ground pattern. *Journal of Comparative Neurology* **520**:2824–2846.  
1425 doi:10.1002/cne.23059
- 1426 **Wolff GH**, Strausfeld NJ. 2015. Genealogical correspondence of mushroom bodies across  
1427 invertebrate phyla. *Current Biology* **25**:38–44. doi:10.1016/j.cub.2014.10.049
- 1428 **Wolff GH**, Thoen HH, Marshall J, Sayre ME, Strausfeld NJ. 2017. An insect-like mushroom body in a  
1429 crustacean brain. *eLife* **6**. doi:10.7554/eLife.29889
- 1430 **Wyatt TD**. 2014. Proteins and peptides as pheromone signals and chemical signatures. *Animal*  
1431 *Behaviour* **97**:273–280. doi:10.1016/j.anbehav.2014.07.025
- 1432 **Yin GL**, Yang JS, Cao JX, Yang WJ. 2006. Molecular cloning and characterization of FGLamide  
1433 allatostatin gene from the prawn, *Macrobrachium rosenbergii*. *Peptides* **27**:1241–1250.
- 1434 **Zbinden M**, Berthod C, Montagné N, Machon J, Léger N, Cheretemps T, Rabet N, Shillito B, Ravaux J.  
1435 2017. Comparative study of chemosensory organs of shrimp from hydrothermal vent and coastal  
1436 environments. *Chemical Senses* **42**:319–331. doi:10.1093/chemse/bjx007
- 1437 **Zbinden M**, Gallet A, Szafranski KM, Machon J, Ravaux J, Léger N, Duperron S. 2018. Blow your nose,  
1438 shrimp! Unexpectedly dense bacterial communities occur on the antennae and antennules of  
1439 hydrothermal vent shrimp. *Frontiers in Marine Science* **5**. doi:10.3389/fmars.2018.00357

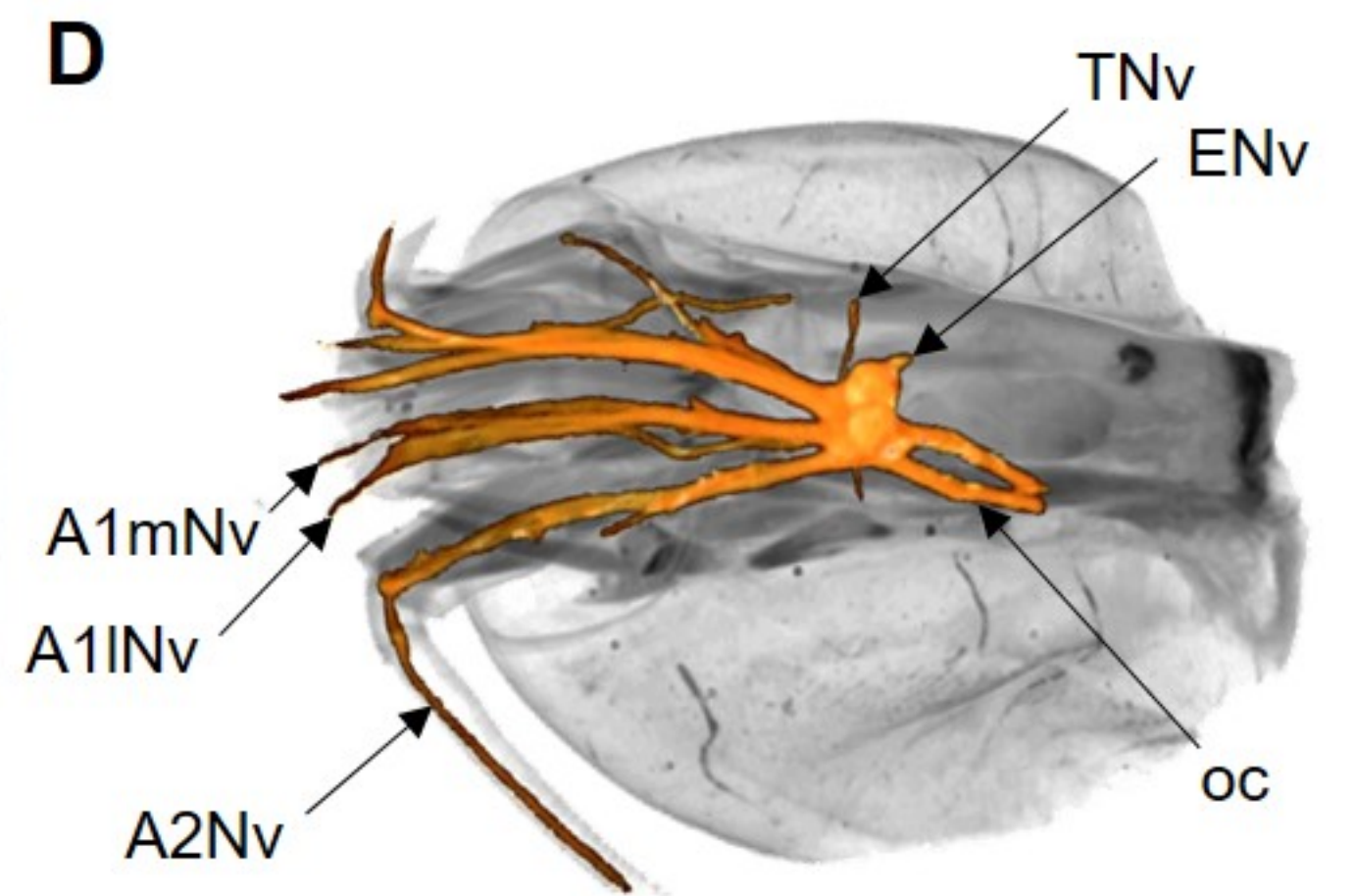
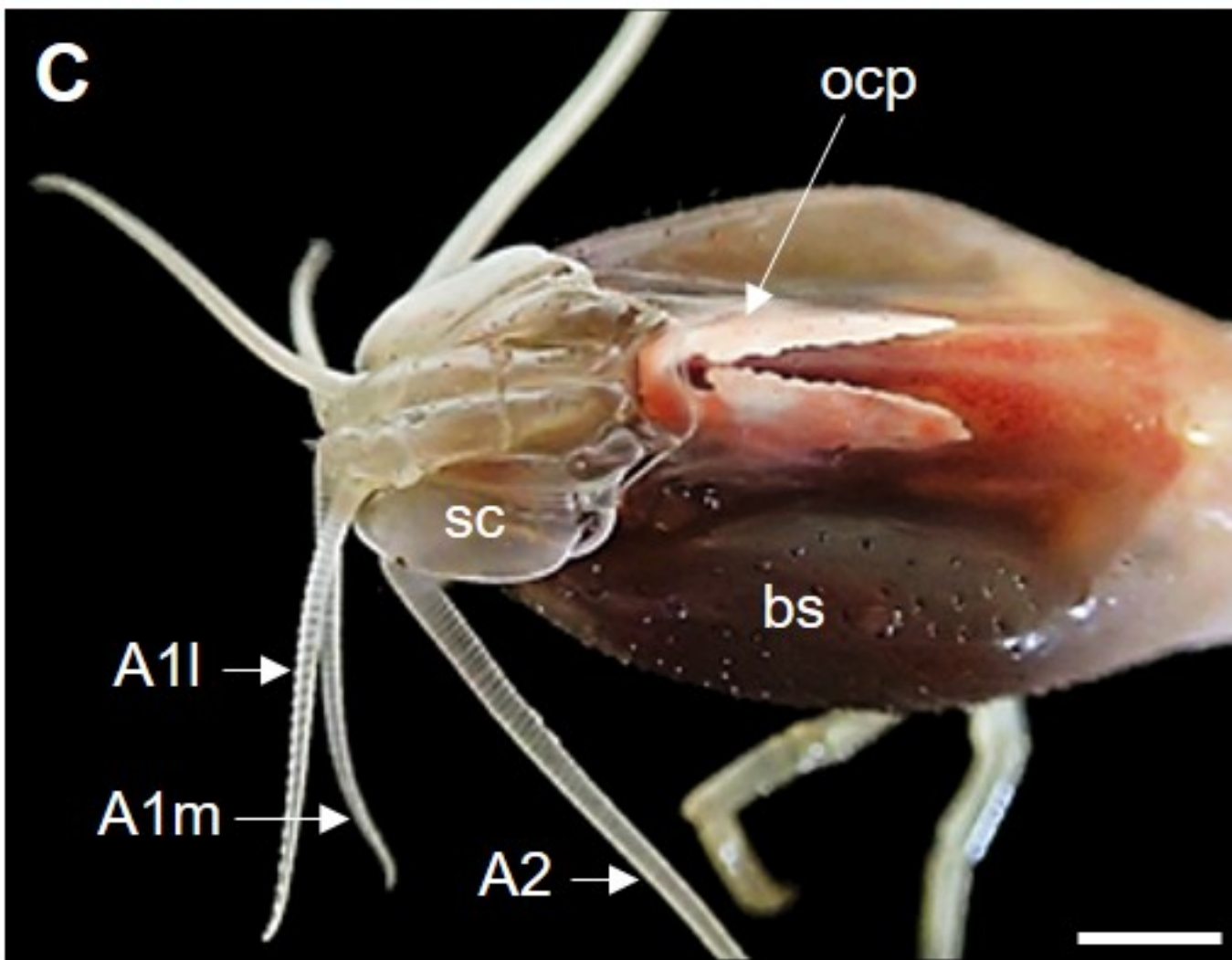
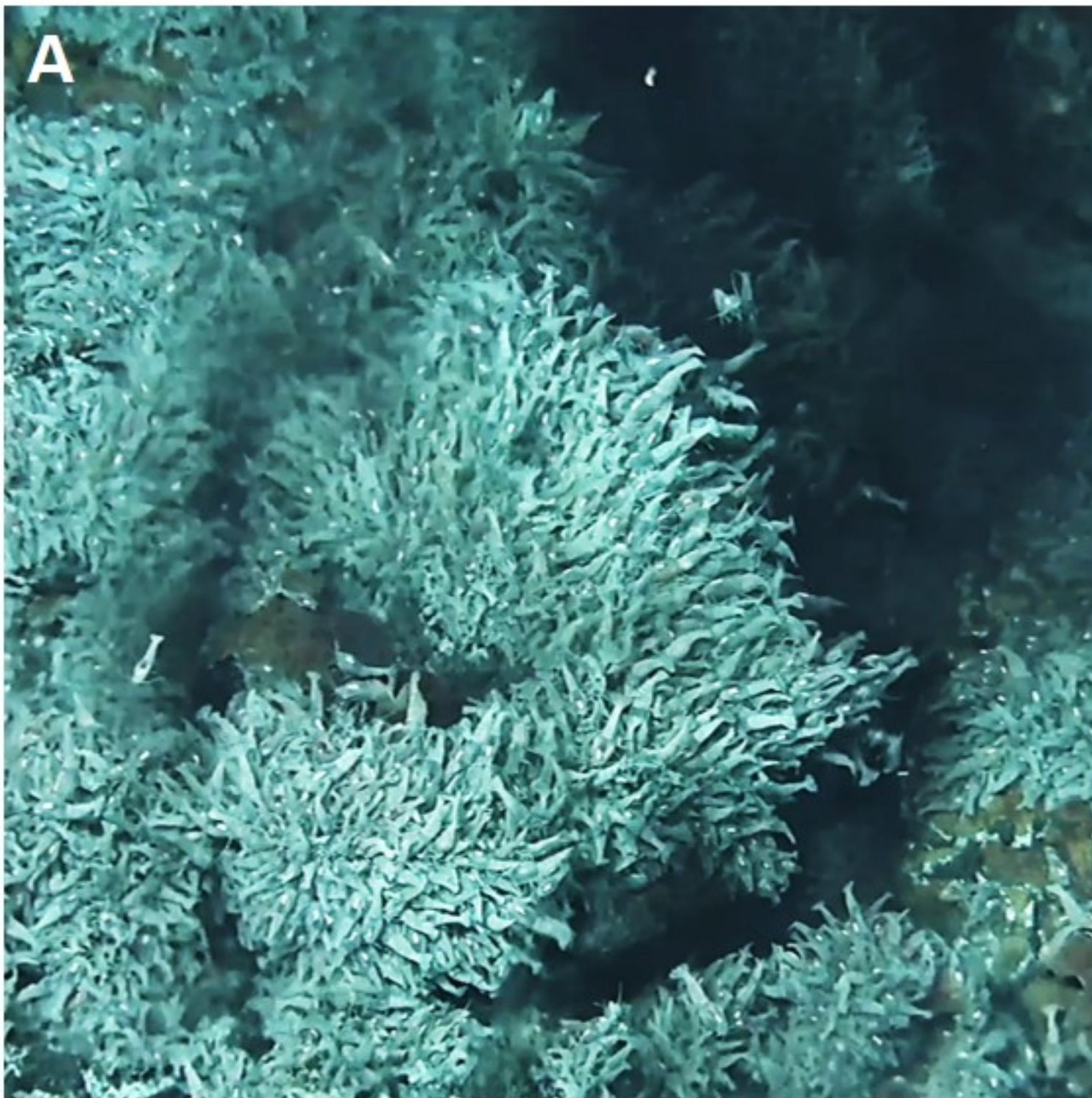
- 1440 **Zbinden M**, Le Bris N, Gaill F, Compère P. 2004. Distribution of bacteria and associated minerals in  
1441 the gill chamber of the vent shrimp *Rimicaris exoculata* and related biogeochemical processes.  
1442 *Marine Ecology Progress Series* **284**:237–251.
- 1443 **Zbinden M**, Shillito B, Le Bris N, de Villardi de Montlaur C, Roussel E, Guyot F, Gaill F, Cambon-  
1444 Bonavita M-A. 2008. New insights on the metabolic diversity among the epibiotic microbial  
1445 community of the hydrothermal shrimp *Rimicaris exoculata*. *Journal of Experimental Marine*  
1446 *Biology and Ecology* **359**:131–140. doi:10.1016/j.jembe.2008.03.009
- 1447 **Zeng Z**, Dai L, Liu Y, Li H, Li Q, Wang J. 2002. Surface microstructures of the antennule of the white  
1448 shrimp *Penaeus vannamei*. *Journal Huazhong (Central China) Agricultural University* **21**:371–378.  
1449

| Species (body length)                    | Aesthetascs  |             | Olfactory neuropils (ON)                                  |  |                   | References  |
|--|--------------|-------------|---|--|-------------------|---|
|  | Total number | Length (μm) | Neuropil total volume (x10 <sup>6</sup> μm <sup>3</sup> ) | Mean glomerular volume (x10 <sup>3</sup> μm <sup>3</sup> ) | Glomerular number |   |
| <b>Leptostraca</b>                       |              |             |   |  |                   |   |
| <i>Nebalia herbstii</i> (1.4 cm)         | -            | -           | 0.1   | 2  | 60                | <a href="#">Kenning et al., 2013</a>  |
| <b>Stomatopoda</b>                       |              |             |   |  |                   |   |
| <i>Neogonodactylus oerstedii</i> (4 cm)  | 80           | 400         | -   | 110  | 70                | <a href="#">Derby et al., 2003</a>  |
| <b>Isopoda</b>                           |              |             |   |  |                   |   |
| <i>Saduria entomon</i> (8 cm)            | 40-60        | 240         | 3   | 34   | 80                | <a href="#">Kenning and Harzsch, 2013</a> ; <a href="#">Pynnönen, 1985</a>      |
| <b>Dendrobranchiata</b>                  |              |             |   |  |                   |   |
| <i>Penaeus vannamei</i> (7 cm)           | 280          | -           | -   | -  | <100              | <a href="#">Wittfoth and Harzsch, 2018</a> ; <a href="#">Zeng et al., 2002</a>  |
| <b>Caridea</b>                           |              |             |   |  |                   |   |
| <i>Palaemon elegans</i> (7 cm)           | 280          | 230         | 120   | 225  | 530               | <a href="#">Zbinden et al., 2017</a> ; this study*                              |
| <b><i>Rimicaris exoculata</i> (6 cm)</b> | <b>206</b>   | <b>170</b>  | <b>56</b>   | <b>155</b>   | <b>370</b>        | <a href="#">Zbinden et al., 2017</a> ; this study                               |
| <b>Achelata</b>                          |              |             |   |  |                   |   |
| <i>Panulirus argus</i> (20-60 cm)        | 3000         | 1000        | 154   | 118  | 1332              | <a href="#">Beltz et al., 2003</a> ; <a href="#">Grünert and Ache, 1988</a>     |
| <b>Homarida</b>                          |              |             |   |  |                   |   |
| <i>Homarus americanus</i> (20-60 cm)     | 2000         | 600         | 141   | 592  | 249               | <a href="#">Beltz et al., 2003</a> ; <a href="#">Guenther and Atema, 1998</a>   |
| <b>Astacida</b>                          |              |             |   |  |                   |   |
| <i>Procambarus clarkii</i> (9 cm)        | 133          | -           | 10  | 20   | 503               | <a href="#">Beltz et al., 2003</a>  |
| <b>Anomura</b>                           |              |             |   |  |                   |   |
| <i>Birgus latro</i> (20 cm)              | 1700         | -           | 375   | 280  | 1338              | <a href="#">Krieger et al., 2010</a>  |
| <i>Coenobita clypeatus</i> (6 cm)        | 519          | -           | 120   | 154  | 799               | <a href="#">Beltz et al., 2003</a>  |
| <i>Pagurus bernhardus</i> (3 cm)         | 673          | -           | -   | 171  | 536               | <a href="#">Tuchina et al., 2015</a>  |
| <b>Brachyura</b>                         |              |             |   |  |                   |   |
| <i>Carcinus maenas</i> (9 cm)            | 200          | 750         | -   | 247  | -                 | <a href="#">Fontaine et al., 1982</a> ; <a href="#">Hallberg and Skog, 2011</a> |

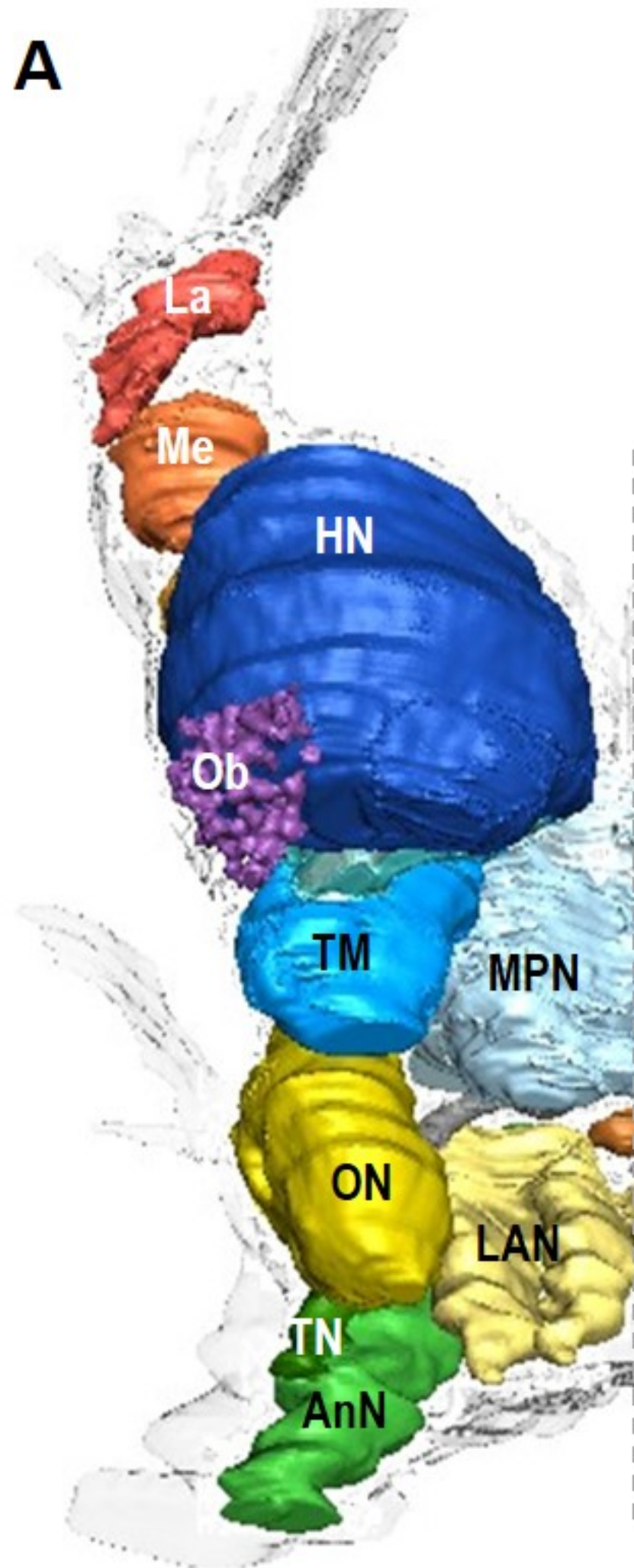
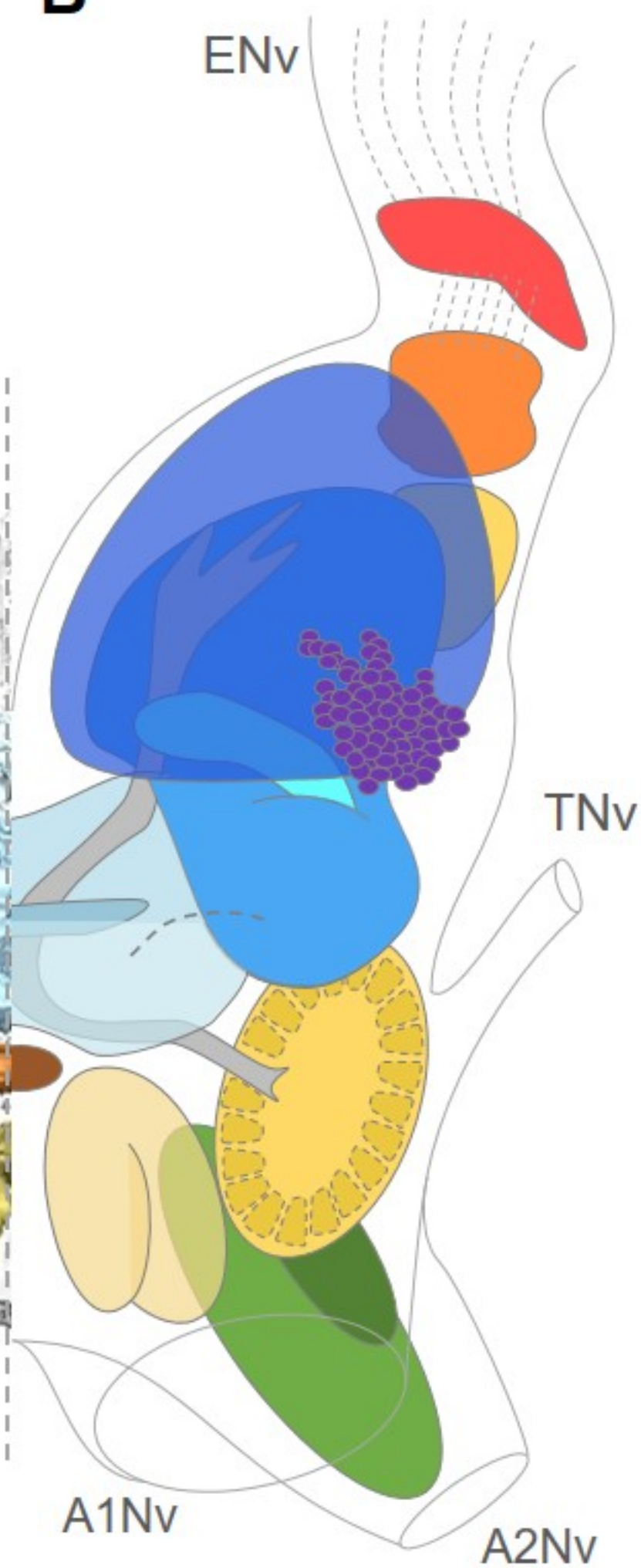
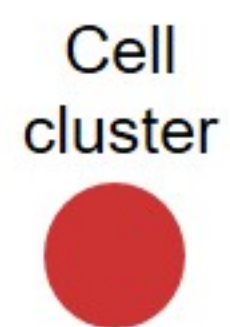
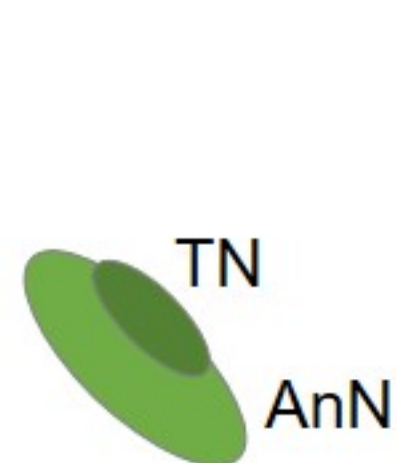
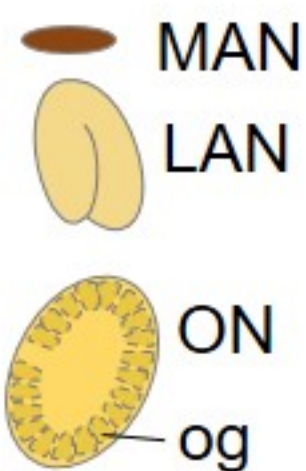
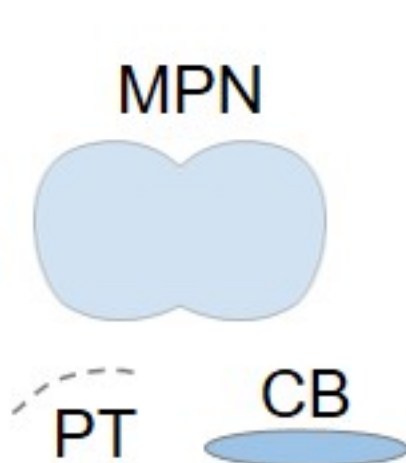
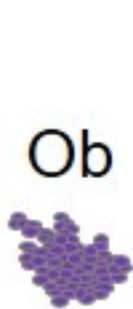
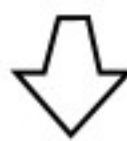
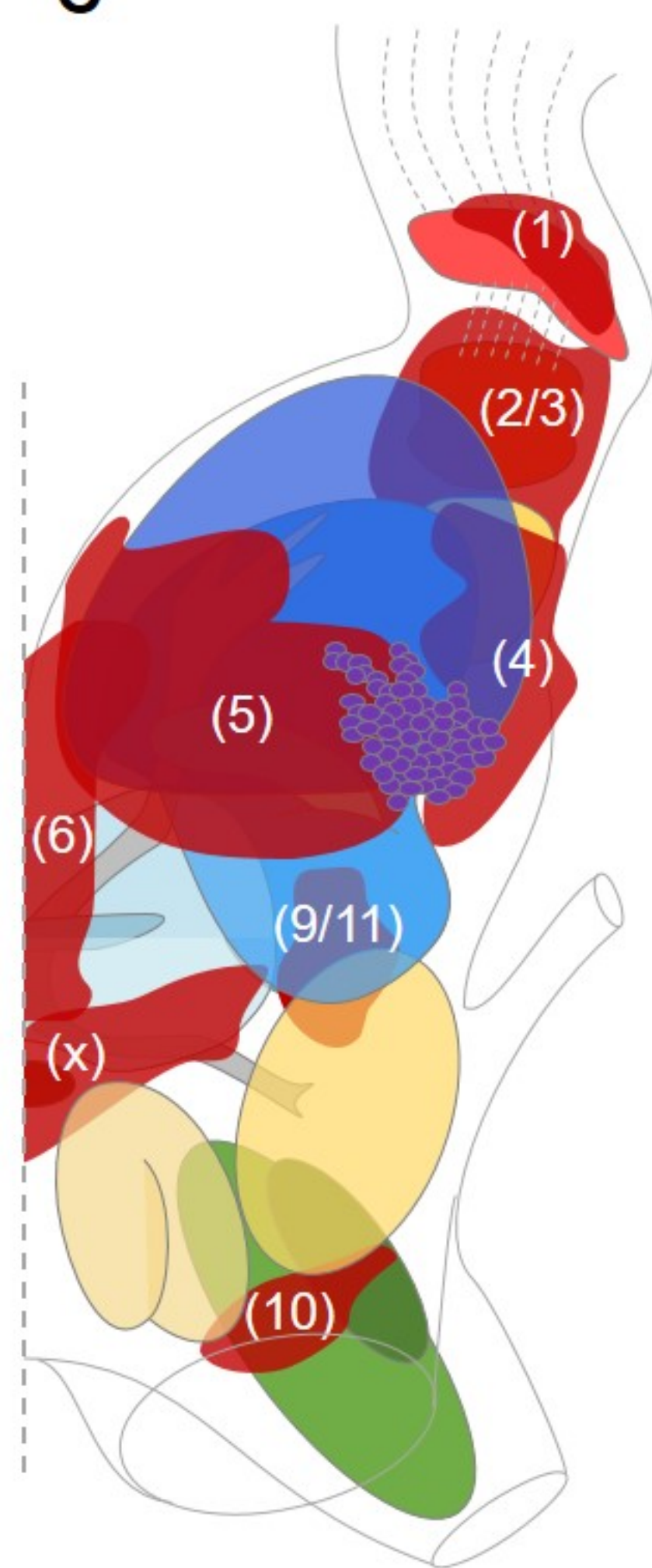
2 **Table 1. Comparative table summarizing characteristics of aesthetascs and olfactory neuropils in several**  
3 **malacostracan species.**

4 Estimates of the animal's body lengths are given for comparison. Carapace width is given for *B. latro* and *C.*  
5 *maenas*, and total length is given for all other species.

6 \* The palaemonid shrimp *Palaemon elegans* was investigated in the present study for comparison, as a species  
7 closely-related to *R. exoculata* among the Caridea family.





**A****B****C**

Visual neuropils

Protocerebrum

Deutocerebrum

Tritocerebrum

